Assimilation of Geosat altimetric data in a nonlinear shallow-water model of the Indian Ocean by adjoint approach.
Part2: Validation and analysis of the assimilated results

by

Eric Greiner (*) and Claire Perigaud (**)

submitted to Journal of Physical Oceanography

February 21, 1995

(*) LODYC, University Pierre et Marie Curie, Casier Postal 100, 4 place Jussieu, 75252, Paris cedex 05, France

(**) Caltech / Jet Propulsion Laboratory, MS 300/323, 4800 Oak Grove Drive, Pasadena, CA 91109, USA

Abstract

This study examines the impact of assimilating Geosat sea level variations over 1986-1988 in a nonlinear reduced-gravity model of the Indian Ocean. The time-invariant simulated sea level is first validated with hydrographic observations performed in the Indian Ocean along non-repetitive transects. The simulated large scale dynamic topography agrees much better with the hydrographic one with assimilation than without. The best agreement is obtained for the initial conditions of the assimilation experiment.

The difference between the yearly-mean dynamic topography determined by assimilation during year 1 (November 1986 to November 1987) and the yearly-mean simulated without data assimilation has a strong signal located south of 109S. This difference is anticorrelated to the one obtained by assimilation during the following year. These differences are not due to wind error. Simulations driven by various wind forcings present the same features over the two years. An analysis of the Throughflow indicates that the major model data discrepancy is due to the lack of connection with the Pacific.

Without assimilation, the equatorial slope in November 1986 is too flat and the center of the southern Southern Gyre is located too far in the south-west. Assimilating sea level variations affects the time-invariant water mass distribution in space and the velocity fields in order to compensate for these deficiencies. It initially reinforces the Wyrtki jet, the westward South Equatorial Current, the southward Somali current, the northward East African Current and the eastward South Equatorial Counter Current. The impact of assimilation on off-equatorial currents lasts for more than a year.

1. Introduction.

Time-invariant ocean dynamic topography is very difficult to assess from

altimetry, because of geoid uncertainty. In absence of geodetic mission or gravimetric observations, the only hope to improve our knowledge of the geoid from altimetry is to improve our knowledge of the time-invariant ocean dynamic topography, via inverse modeling (Roemmich and Wunsch, 1982), or via assimilation into dynamic models simulating the oceanic circulation (Dombrowsky and De Mey, 1992).

Large-scale low-frequency sea level variations in the Indian Ocean simulated by a shallow-water model are highly dependant on the mean state of the ocean. Simulated annual and interannual variations agree with Geosat much better when the model has been run with all the nonlinear terms than without (Perigaud and Delecluse, unpublished manuscript). This is why it is possible via assimilation of observed sea level variations to optimize the time-invariant dynamic topography that provides the minimal model data misfit.

The method and a couple of experiences where Geosat sea level variations were assimilated in the shallow-water model are presented in part 1 of this study (Greiner and Perigaud, 1994, further referenced to as GP94). In these experiences, the shallow-water model is a fully non-linear model, with a coarse resolution (2° by 20), an initial upper layer thickness of 200m and a relative density ratio of 3x10-s. It covers the Indian Ocean north of 42*S with closed lateral boundary conditions everywhere. The model is expected to have some skill only north of 20°S, the variations being damped in the southernmost band. The model is driven by FSU wind stress over 1985-1989, after six years of spin-up from rest with the 4-year averaged monthly wind stress. Wind stress have been derived from FSU pseudo-stress, using a constant drag coefficient equal to 1.3 x 10-3. Geosat observations have been assimilated north of 20% and during one year starting on November 15 1986. This year is further referenced to as "year 1" and the following year as "year 2". The assimilation was performed with the adjoint technique by optimally estimating the initial conditions only

sea level affects the velocity fields simulated by the model. There is little observations of current available in the ocean (for a review, see Schott, 1992). Current meter data provide some insight for a particular time on the vertical structure of the currents. They have highlighted the need for several baroclinic modes of variations (Fieux et al, 1986). It is well known that several baroclinic modes are needed to adequately simulate the equatorial current variations, even in the upper ocean (see e.g. Gent et al, 1983). With a shallow-water model, we ignore these higher modes of variations and provide a very simple synopsis of the circulation in the upper layer. A synoptic view of the surface currents can be derived from ship drifts (Cutler and Swallow, 1984) or drifters (Molinari et al, 1990). These observations provide climatologic information. Their coverage in space and time over the past decade has not not been dense enough to provide anomalies over eve?< specific year. So, we are not able to validate the simulations of currents other than by comparison with climatology. We will see that the impact of assimilation on surface currents is very dependant on the year. Nevertheless, the current fields are modified by assimilation in a wind-driven shallow-water model and are consistent with the simulated thermocline depths. Confidence is gained in the assimilated results if the latter are validated with independent observations.

This paper is organized as follows. In section 2, the impact of assimilation on the thermocline field averaged over year 1 is presented and validated with results derived from hydrographic observations. In section 3, we present the mean thermocline field estimated by assimilating Geosat over year 2 and examine the changes between the two yearly-averaged surfaces. in section 4, we analyse the impact of assimilation on the current velocity fields.

2. Mean dynamic topography over year 1.

2.1 Impact of assimilation over year 1.

In this section, the thermocline depth simulated by the shallow-water model (with or without assimilation) is averaged over the year starting on November 1986. Its value averaged over the model domain north of 20% (158m with or without assimilation) is retrieved and the relative surface is converted into sea level, using the density ratio assumed in the model. The yearly-mean surface is presented in Figure 1 without assimilation (top) or when Geosat data have been assimilated in ASS2 experiment (bottom).

With assimilation, the strong topographic gradient corresponding to the mean axis of the South Equatorial Current (SEC) is more tilted towards the South-West and its path turns South of the Saya de Malha bank. In the East, the northern border of the southern gyre reaches 100ºE- 139S with assimilation, instead of 92^{Q}E-19% without. The large cyclonic gyre north of it, is stronger and its center is located closer to the middle of the ocean at about 70^{Q}E-10?$. Between 5*S and 5*N, the topography is flatter. A cyclonic gyre is present north of the equator around the Maldives with a center at about 70ºE-5ºN. In the Arabian sea and the Bay of Bengal, the mean circulation presents a pair of strong cyclonic and anticyclonic gyres. Let us examine first if these results can be validated with independent observations.

2.2 Comparison with observed surface dynamic height.

Our objective is to validate the ocean dynamic topography at a given time. This quantity is not provided by altimetry because of geoid uncertainty. Altimetric data which were assimilated provide information only for the variable part of the ocean topography. Because of our modeling approach, we are

interested in the large-scale gradients of the topography, not the mesoscale. Using *in situ* data to validate these gradients simulated by a shallow-water model is a difficult exercice. Besides the fact that model and data do not have the same coverage nor resolution in time and space, we are limited because there is no direct measurement of what the model simulates. Our shallow-water model simulates the signal contained in the first baroclinic mode only. Reality is a lot more complex, especially for the time-invariant component of the topography. This is why two different signals derived from XBT are used below. One is the surface dynamic topography derived from TOGA XBT data provided by Dr Rebert (see Rebert, 1993). Let us call it "$hdyn_{XBT}$". The other one is the analyzed depth of the 20º isotherm provided by Dr Smith (see Smith et al, 1991: Smith, 1995). Let us call it "D20". A big advantage of D20 data set is that it is a gridded field and the difference between model and data can be taken at each grid location and time. A big advantage of the $hdyn_{XBT}$ data set is that data are raw, they do not contain as D20, *a priori* information about the ocean topography.

Although we had acquired the TOGA XBT data in the Indian Ocean for the year 1987 long ago, we had not yet been able to compare them with Geosat because altimetry provides only the variable part of the oceanic signal. The XBT network in the Indian ocean does not have a good enough repetitivity to provide an accurate estimate of sea level variation. The XBT data set available during Geosat consists of irregularly spaced data. One of the most regularly sampled transects is represented by "*" in Figure 1. Data were binned and averaged on two degree square boxes along this transect every month when data were available. The salinity was estimated at each square box from the Levitus seasonal climatology (Levitus, 1982). The surface dynamic heights were computed relative to the deepest level (450m) and relative to 150m (as it is close to the averaged depth simulated by the model). Because the sections have large

irregular gaps, we chose not to apply any spatial smoothing techniques. Surface dynamic heights relative to 150m are then plotted relative to their mean in time and space along this transect which is equal to 175cm (Figure 2).

In order to compare with the model output, we took the corresponding monthly means of the simulated thermocline fields (with or without assimilation), extracted the simulated values along the hydrographic section, retrieved the spatial and temporal mean value of this section (155m with or without assimilation), and converted the thermocline depth into sea level using the model density ratio.

Figure 2 shows that hydrographic plots have a rough topography with strong mesoscale signals. These features are not present in the simulations, whether Geosat has been assimilated or not. This is not surprising as the model has a coarse spatial resolution and does not catch the complex reality, which has been observed at specific locations and times by the XBT. We concentrate instead on the large-scale signal.

Figure 2 shows that model and XBT data disagree South of 15ºS. The XBT plots indicate a slope reversal corresponding to the signature of the South Equatorial Current north of 15*S and an eastward flow South of it. This happens because the surface dynamic height has been computed relative to 150m only. The surface dynamic topography relative to 450m reverses further south, at 18*S, close to where the slope of the 20°C isotherm reverses (see section 2.3). The choice of the level of no motion is the first source of persistant error in the computation of a surface dynamic height at a given time. However, the amplitude of the signal relative to 450m north of 15QS is much larger than relative to 150m, whereas the latter is close to the one simulated by the model.

Figure 2 shows that assimilation has improved the agreement with hydrography. With assimilation, the model performs much better in simulating the slope between 5°S and 10ºS in January 1987, between 5*S and 15*S in March

1987 and to a lesser extent, the slope between 10°S and 15'S after May 1987. The impact of assimilation is the largest in January 1987 all along the transect. The sea level difference between 15% ant 5ºN is 9 cm for the model without assimilation. It is 25 cm for the XBT data or for the model with assimilation. The improvement is similar for experiments ASS 1 and ASS2. Both correspond to experiments where initial conditions have been optimized. This is why the best agreement is reached for the transect which is the closest to November 1986.

In terms of temporal variation, the agreement between hydrography and model is also improved by assimilation. This was not *a priori* certain, because Geosat contains some errors (which were accounted for in the assimilation), the model contains other errors (which were not account for), and the XBT also contain other errors. The spatial averages of the hydrographic sections fluctuate in time as the ones simulated by the model with a positive correlation (0.27 without assimilation, 0.69 with ASS1 and ASS2). The biggest change is a drop of 4 cm between March and August, which takes place for the ASS 1, ASS2 and XBT plots, whereas the simulated plot without assimilation rises by 1.5 cm. The hydrographic values, however, may be biased by the fact that the XBT plots do not have the same resolution along the track each month. So let us look at the analyzed depth of the 20°C isotherm.

2.3 Comparison with depth of the 20ºC isotherm.

Data consist of analyzed fields and error fields of the 20ºC isotherm depth on a regular grid with 2 degrees in longitude, 1 degree in latitude and 10 days (Smith, 1995). Let us start our comparison along the XBT transect defined above, as the D20 error is minimal there.

Let us first examine the signals along this transect. We extracted the D20 signal along the transect and overplotted the simulated thermocline depth without removing any mean to any plot (Figure 3). The success of assimilation is quite

impressive. For each transect between November 1986 and August 1987, correlation is improved and rms difference is reduced (table 1). Overall, the most performant assimilation experiment is ASS2. For the months of August to October 1987, the optimization of the initial conditions only (ASS1) has not improved but degraded the agreement. The additional optimization of the yearly-averaged topography (ASS2) gives a better agreement than ASS 1, but ASS2 still does not do as well as the model without assimilation.

The D20 fields were then systematically compared with the model outputs for each month all over the Indian Ocean north of 20ºS. Their differences are smaller with assimilation than without, for all months before April 1987 (table 2). Map differences are presented for the initial conditions in November 1986 (Figure 4). If we consider D20 as the ground truth, Figure 4a indicates that the model without assimilation is simulating a thermocline which is too shallow south of 10*S and too deep along a V-shape path going from Western India to Kenya and all along the South Equatorial Counter Current to Java. The equatorial slope simulated without assimilation is flat, whereas D20 is thickening by 22m between 65°E and 90ºE. Figure 4b has similar patterns, showing that assimilation tends to correct for this model deficiency. These two figures are correlated by as much as 0.88. Patterns of Figure 4a and 4b differ in the Bay of Bengal, the exit of the Gulf of Aden and around 105QE-18*S. Little can be expected from these regions where model and Geosat are inconsistent, or where the XBT coverage is poor. Another interesting common feature was found by plotting these differences as a function of time along zonal sections in the southern band (along 10°S, 15QS, 20%). These differences (whether it is relative to D20 or to ASS1) propagate westward as Rossby waves. This is also the case for the simulations without assimilation (Perigaud and Delecluse, 1992).

This comparison supports that assimilating altimetric data is successful in reducing the discrepancy between model and reality observed with hydrographic

data. This success is valid for the low-frequency variations, and even for the large-scale gradient at a given month. On the other hand, it shows that optimizing the initial conditions degrades the model skill in simulating the reality after 9 months of assimilation. Optimizing the yearly-averaged topography cannot compensate for this degradation. This is consistent with the results of GP94. We have seen that the optimal control obtained by assimilation over year 1 in experiment ASS2 leads to an increase of the misfit between Geosat and the model for the following year. This is why we run below an ASS2 experiment performed on year 2.

3. Dynamic topography over year 2 and changes between year 1 and year 2.

3.1 Results from assimilation of Geosat over year 2

A similar experiment to ASS2 over year 1 was run the following year in order to determine the optimal control over year 2. The yearly averaged dynamic topography is presented without assimilation and with ASS2 for year 2 in Figure 5. With ASS2, the mean topography has stronger gradients, especially in the Bay of Bengal and on the east side of the equator, but changes along the South Equatorial current are not as drastic. As in GP94, model and data are inconsistent within our *a priori* data errors, in the Bay of Bengal and East of 110ºE. The reduction of discrepancy between Geosat and model is similar to the previous year. The rms difference between the observed and simulated thermocline variations is reduced from 20m without assimilation to 16 m with ASS2. Corresponding values for year 1 are 21m and 16m (see GP94). We also checked that the results over year 2 can be validated with D20 as above. However, the impact of assimilation in the South is not as strong as for year 1. In

particular, the difference between the model without and the model with ASS2 is not as large in November 1987 as in November 1986. This is confirmed by D20.

3.2 Changes between year 1 and year 2.

Compared with year 1, the mean dynamic height over year 2 is lower in the 20°S-10% band and higher in the whole eastern part of the Indian Ocean. Such a change is found in the simulations without assimilation (Figure 6a). This latter change is driven solely by the wind. It has a spatial variability (2cm) which is twice smaller than the one simulated with ASS2, when ASS2 has been performed over each year separately (Figure 6b). This latter change is in excellent agreement with Geosat (see GP94, Figure 8). The Geosat and ASS2 maps have the same variability (4cm). Geosat and simulated maps are spatially correlated by 0.67 without assimilation and by 0.94 with ASS2. Geosat and ASS2 changes between year 1 average and year 2 average are characterized by a sea level rise in the central domain (10ºS-1 ON), and a drop north and south of it. Comparison between simulations and observations (Perigaud and Delecluse, 1993) has shown that the interannual change could not be fully explained by the wind change.

The correction brought by assimilation (Figure 7) is a signal larger than the interannual change driven by wind only. It is striking that the corrections for the 2 years are positively correlated north of 5ºN, whereas they are negatively correlated south of 8°S. In addition, the correction south of 10QS is much stronger over year 1 than over year 2: the maximum tilt over year 1 is +18 cm between (20°S, 90ºE) and (1 OO°E, 10°S), whereas it is only -8cm between (20ºS, 85ºE) and (90ºE, 13QS) over year 2. These are important features which we need to understand. Both maps correspond to a signal which is missed by the model without assimilation, and recovered by assimilation. Among the various error sources, one could be wind uncertainty.

3.3. Changes due to winds

With a 3D Primitive Equation model over the Indian Ocean, Anderson and Barrington (1993) have compared simulations forced by different winds and have highlighted the importance of wind uncertainty. Here, we use shallow-water simulations driven by ECMWF winds instead of FSU winds, in order to have an estimate of a misfit due to wind inaccuracy only. For both runs, we used simulations driven by winds from January 1985 to December 1988, after six years of spin-up by the monthly winds averaged over 1985-1988. For ECMWF, we used the 10m winds converted into wind stress with the same drag coefficient as for FSU winds. As found over the tropical Pacific Ocean (Chao et al, 1993), the ECMWF winds are systematically much weaker than the FSU winds. This has drastic consequences on the shallow-water simulations over the Indian Ocean. Due to weaker wind strength, the dynamic topography driven by ECMWF has a much weaker meridional gradient across the South Equatorial Current. This implies that after the spin-up, the model driven by ECMWF simulates a thermocline at 190m on average north of 20°S, which is deeper by 30m than the thermocline driven by FSU (Figure 8). Because the model driven by ECMWF has such a flatter time-invariant topography, sea level variations driven by ECMWF winds are close to the linear ones. In addition, the FSU and the ECMWF runs have very different sea level variations in the 10%-20% band (see Perigaud and Delecluse, 1993). So *a priori*, it is quite possible that assimilation has compensated for errors in the FSU wind more than anything else. If this is the case, the yearly averaged difference between the 2 runs should present some similarities with the maps presented in Figure 7.

The simulated dynamic topography was averaged over year 1 and over year 2 for the FSU or for the ECMWF runs. As explained above, the yearly averaged dynamic topography north of 20% (over year 1 or over year 2), is 10 cm higher for the ECMWF run than for FSU. The differences between the two runs are

presented in Figure 9 for year 1 or year 2, both relative to 10cm.

For both years, the two maps present similar patterns, corresponding to a zonal tilt higher with FSU on the eastern domain than with ECMWF. This is consistent with the difference found in the mean wind-stress curls (not presented here). Over year 1 and year 2, the line of zero wind-stress curl for ECMWF wind is located more south and more tilted to the northeast than for FSU winds.

The other differences are on a smaller scale and are mostly located in the western Indian Ocean. FSU simulations present a strong anticyclonic eddy located at 3*S along the East African coast south of the Equator. This eddy is not present in the simulations driven by ECMWF (Figure 9). In the simulations driven by FSU, it is built up by nonlinearity, as it does not show up in the linear FSU simulations.

Another discrepancy between ECMWF and FSU simulations is located in the northern Arabian Sea. There, the yearly-averaged topography is characterized by a pair of anticyclonic and cyclonic eddy corresponding to the signature in the annual mean of the Great Whirl and of the Arabian upwelling respectively. The location of such features is highly dependant on the wind-stress curl in summer. The difference between the ECMWF and FSU simulations is persitant over the two years and is consistent with the wind features. In summer, the FSU wind stress curl is stronger and its zero line is located to the North of the ECMWF one.

Comparing Figure 7 and Figure 9 indicates that wind error is a source of discrepancy between model and Geosat. Assimilation has corrected for it mostly in the western Indian Ocean. However, wind error does not explain the largest correction which took place in the 10^{Q}S-20^{Q}S band in year 1.

3.3. Comparison with climatology

We computed the anomaly relative to the 1985-1988 climatology for the

sea level derived from D20. Yearly-averaged anomalies are presented in Figure 10 for year 1 or for year 2. The anomaly in the 10'S-20'S is much more intense for year 1 than for year 2. Sea level anomaly over year 1 is higher by 10 cm at (90ºE-1 5'S) than climatology, whereas very little anomaly is found over year 2. This is in agreement with the El Nino signal described in Tourre and White (1995). We then mapped the corresponding anomalies simulated by the model driven by FSU over 1985-1988 after spin-up. Simulated maps are positively correlated with D20 for both years, the anomaly in the South is stronger for year 1 than for year 2 as in D20. However, the amplitude is much smaller than for D20 (the maximum simulated change for year 1 is +3 cm). Year 1 is a strongly anomalous year. The anomaly is not only driven by the wind over the Indian Ocean. It is likely that part of it is influenced by the excess of warm waters that penetrated in the Indian Ocean via the Throughflow.

Using the 1985-1988 model simulations, we computed the transport between (11 0ºE-20ºS) and (1 10QE-9QS), which is close to the section between Indonesia and the Northwestern tip of Australia. The simulated transport (Figure 11) corresponds to the one driven by the winds over the Indian Ocean only. The model boundary (along the isobath 200m) does not allow inflow from the Pacific. So the model simulates a mean flow which is nil. The climatologic run after spin-up is dominated by annual fluctuations corresponding to an increase of westward transport from late winter to late summer. These are consistent with observations (Meyers et al, 1994a) and with simulations (Kindle et al, 1987). The model simulates weak anomalies, with a minimum westward transport in April 1986 and a maximum in December 1988. The Throughflow observed by (Meyers et al, 1994b) also presents weak anomalies over year 1 and year 2, but it has a very strong minimum in June 1985. Then, the total transport was even eastward. An estimate of the transport variations observed by Geosat can be derived by making the geostrophic approximation. Based on model simulations

(Figure 11), this approximation is quite valid for this section. The transport derived from Geosat variations is presented in Figure 11 over year 1 and 2 (we do not have the estimate in 1985). Geosat and simulated transports have similar annual fluctuations. Interestingly, Geosat indicates that the westward transport was slightly stronger over year 1 than over year 2, in particular there is an anomalous inflow in December 1986. This is also the case in the observed transports (Meyers et al, 1994b). We checked that the transport simulated with ASS 1 is very close to the one without assimilation. This is because the model assumes a closed boundary with the Pacific, and this is a region where model and data are inconsistent.

With closed boundary conditions, the model cannot reproduce variations of the Throughflow, whether data are assimilated or not. Nevertheless, the assimilation of Geosat variations in the interior domain has probably introduced in the 10ºS-20ºS band away from the eastern boundary, the signature of the Throughflow anomalies which took place prior to November 1986. It is recovered by assimilation in the shallow-water model as a first baroclinic signal. Let us now examine the impact of assimilation on the current fields in the interior domain.

4. Impact of assimilation on the velocity fields

The biggest impact of assimilation takes place over year 1, especially in winter 1986-1987, when there was a strong anomaly. There is no velocity current data available at that time to validate the assimilated fields. We can only compare with the simulated fields published in the literature or observed climatologic currents. However, based on comparison with XBT data, the model simulates more realistic thermocline gradients, especially in winter 1986-1987. So, it is interesting to examine the impact of assimilation on the velocity fields at

this time. Past 9 months, the optimization of the initial conditions does not allow to simulate thermocline gradients which are more realistic. Nevertheless, we examine the simulated currents between November 1986 and November 1988, because it is important to understand how improving the initial conditions modifies the velocity fields over a long time.

4.1 Initial conditions

The velocity fields simulated on November 15, 1986 are presented in Figure 12, without assimilation or with ASS1. The velocity fields simulated with ASS 1 or with ASS2 are very similar.

Assimilation has considerably affected the. flow along the Equator. Without assimilation, this flow is eastward only west of 70ºE. With assimilation, it is strong and eastward all across the ocean. November is the time of the year when we expect the Wyrtki jet (1973) all along the equator. Based on climatology (Cutler and Swallow, 1984; Rao et al, 1989), the Wyrtki jet is expected to be as strong as the flow simulated with assimilation. According to climatology, the flow simulated with assimilation is thus more realistic. One must not forget however, that the equatorial currents have strong interannual oscillations (Anderson and Barrington, 1993). The one simulated with assimilation is clearly consistent with the thermocline field observed in November 1986. We have seen in section 2 that the model was then simulating a flat equatorial slope without assimilation, and that the model with assimilation recovers a rising slope from 65ºE to 90ºE, which is also present in the D20.

Assimilation has two effects on the meridional component. One is to stop the southward Somali current North of the equator. The other one is to generate a northward cross-equatorial flow between 70ºE and 90ºE. Let us now examine the impact of assimilation on the velocity field past the initial conditions.

4.2 Circulation of the southern cyclonic gyre

Water mass transport in the upper layer of the ocean was computed for various sections across the main currents of the Indian Ocean, the South Equatorial Current (SEC), the currents north and west of Madagascar, the South equatorial Counter Current (SECC), the Somali current and various equatorial sections. Transports were computed for the model without assimilation, and for the various assimilation experiments. We present the results for experience ASS1 over year 1, meaning that the model is run for two years, starting from the optimal initial conditions which have been determined by assimilation ASS 1 over year 1 only.

Two sections 10' wide are presented across the SEC (Figure 13a and b). The impact of assimilation is very strong there. Initially, assimilation has increased the SEC transport by a large factor. This factor varies between 1.5 and 2 depending on the location, the strongest impact being in the East between 90ºE and 100'E. With time, this initial kick decreases and the SEC becomes weaker and weaker. It becomes weaker than the SEC simulated without assimilation after July 1997 at 90°E, after October 1987 at 75ºE. The time after which the SEC with assimilation becomes weaker than the SEC without assimilation, increases from East to West. This is consistent with the results found in section 2. The correction brought by assimilation (as the difference between model and D20) is propagating westward as Rossby waves. Note that for all SEC sections, the annual and sub-annual variations with or without assimilation are highly correlated. Similar variations were found by Woodberry et al (1989). These variations are driven by the wind, whereas the strong interannual drift is due to ASS1 .

The increase of westward current can be felt as far as North of Madagascar . Currents are quite strong at Cape Amber, the transport reaches

almost 10 Sv for a section 2* wide only (Figure 13c). Annual variations of transport 'simulated without assimilation agree well with the ones found in models (Kindle and Thompson 1989, figure 8) or with *in situ* measurements in 1985 (Schott et al., 1988, figure 4a). The initial impact of assimilation is a doubling of transport to the West. The increase of transport lasts past the period of assimilation, for the entire two years.

Similarly, the SECC transport across 2°S-8°S at 50°E is increased to the East for the entire two years (Figure 13d). Note that for the two latter sections, annual, semi-annual and interannual components simulated with or without assimilation are highly correlated. These oscillations are wind-driven, whereas the impact of ASS 1 is a systematic bias over the two years. We checked with several other sections, that the entire circulation of the southern cyclonic gyre (the SEC-EACC-SECC-Java Current loop) is intensified by assimilation. In particular, sections perpendicular to Java-Sumatra show that instead of being northward as expected in November 1986, the transport is southward and feeds the SEC. Initially, the cyclonic circulation is intensified dominantly in the East (Java current and SEC in the East). Past July 1987, it is intensified only in the West.

4.3 Meridional Circulation in the West.

Figure 13e is a 20° wide equatorial section bounded on the West by the African coast. The northward transport peaks are entirely driven by the wind, with one peak in September 1987 and the other one in September 1988. They are present with or without assimilation. Summer peaks of similar amplitudes are also found in the upper 100m in observations (Schott et al, 1990). Initially and for the two first months, assimilation has reversed the direction of transport, the flow with assimilation being to the South. Past April 1987, the current with assimilation is still southward whereas the current without assimilation is

northward. This is consistent with an increased feeding of the SECC required by assimilation as explained above. Note that the peak of southward transport simulated without assimilation in February 1987 is not present with assimilation. The assimilation impact dominates the wind driving at this time. It is striking however, that there is no more impact of assimilation after July 1988, when the strong summer monsoon wind blows.

Figure 13f is a section across the Mozambic channel from Madagascar to Cape Amber. Except for the first. 2 months, both signals have very similar variations, with intraseasonnal oscillations close to 50-70 days and a decreasing trend over the full two years. Intraseasonal oscillations have been found in reality (Schott et al, 1988; Swallow et al, 1988) and in other shallow-water model simulations (Kindle and Thompson, 1989). The interannual trend is wind-driven, as it is present with or without assimilation. The minimum flow in 1988 is in late November, as found in climatologic simulations (Woodberry et al. (1989) see their Figure 9). Simulations in 1987 have a minimum in April 1987 which is very anomalous. With or without assimilation, there is a strong mean northward transport during the two years. It is interesting to note that this is not the case for other shallow-water model simulations (Woodberry et al, 1989). Their model, forced by climatologic winds and with open boundary conditions at 25*S and with the Pacific, simulates a mean southward flow. A mean northward flow is present in our simulations, whatever the year or the wind used. Assimilation does not decrease this flow, but increases it. This is consistent with an increased feeding of the SECC and an intensified cyclonic circulation in the West. The initial kick is tremendous during the first 2 months. The transport is 25 Sv with ASS 1 and 8 Sverdrup without.

Figure 13g is a section perpendicular to the Somali coast at 9*N, as defined in Woodberry et al. (1989). Simulations past April 1987 are very similar with or without assimilation. There is a peak to the north in September and a peak to the

south in March 1988. This is very sire: lar to the climatologic transport estimated by Woodberry et al. (1989). Assimilation has increased the amplitude of the peaks. As seen in section 3, this can be due to errors in the strength or the location of the wind stress curl. Before April 1987, assimilation has increased the transport to the South.

Thus the Somali current, the cross-equatorial current and the EACC, all have been corrected by assimilation in order to feed more the SECC during at least 6 months.

4.4 Circulation along the equator and in the Bay of Bengal

We plotted various sections across the equator and they all have an increased flow to the East initially. This corresponds to the increased Wyrtki jet examined in Figure 10. However, this initial increase does not last long. This is because it takes less than a month to an equatorial Kelvin wave to travel from Africa to Indonesia with a 250 cm/s speed. This initial perturbation is partially damped, partially reflected into Rossby waves at the eastern boundary. The signal along the equator forgets very shortly the initial kick and responds instead, to wind variations. In order to see an impact of assimilation past one month, we present a section not centered at the equator.

Figure 13h is a section at 80°E located South of India from the equator to 3*N. Past April 1987, this transport is dominated by the semi-annual oscillations of the W yrtki jet driven by the wind. Before April 1987, the semi-annual regime was disturbed by assimilation in Fall 1986. Between December 1986 and April 1987, the flow with assimilation is westward. This may be surprising as we have seen that the current simulated with ASS 1 on November 15, 1986 is eastward. This is because the eastward equatorial flow induced by assimilation does not last long and because north of the equator, assimilation creates a westward flow in Fall 1986. This flow has the same sign as the one induced by the exchanges

between the Bay of Bengal and the Arabian sea.

Assimilation induces an initial outflow from the Bay of Bengal into the Arabian sea of 6 Sverdrup measured at 78*E and between 3°N and 6*N. This initial impact lasts up to January 1987 when simulations with or without assimilation become very similar. Variations are dominated by wind reversals with a strong annual and semi-annual component. Flow is westward in winter and eastward in summer. This is in agreement with observations and simulations (Schott et al, 1995). We plotted various sections in the Bay. The impact of assimilation can be strong during year 1. We know that model and data are inconsistent in the Bay. Geosat contains signals which assimilation cannot correct for in a first baroclinic context. The interesting results in the Bay is that past year 1, there is very little difference between simulations with or without assimilation, not even north of 10*N. There is no long-term impact of assimilation as found south of 10°S. Variations in the Bay simulated by a shallow-water model are driven by local winds or remotely driven by equatorial processes propagating alongshore as coastal Kelvin waves and radiating back to the west as Rossby waves (Potemra et al, 1991; McCreary et al, 1993). Having no long-term impact on the equatorial flows, assimilation has no long-term impact on the Bay of Bengal which is locally or remotely wind forced.

This analysis illustrates that assimilation corrects for equatorial adjustment much - must faster than for the off-equatorial one. The time required for the reestablishment of the tilted equatorial slope is only 1 month whereas the adjustment of the cyclonic southern gyre is not finished after two years. Long-term trends in the northern basins are not as prominent, because variations are overly dominated by local winds or equatorial remote winds.

5 Discussion.

Assimilation of Geosat variations in a nonlinear shallow-water model driven by FSU winds has modified the simulated thermocline and velocity fields. We compared the assimilated thermocline depth with *in situ* observations. Simulations with assimilation agree a lot better with reality than without assimilation for winter 1986-1987. The biggest impact of assimilation is located south of the equator. On averaged over year 1, assimilation deepens the thermocline in the southeastern tropical Indian Ocean. The maximum yearly averaged change is 30 m centered at 100ºE-12*S. Assimilating Geosat over the following year has a smaller impact, which is a thermocline shoaling of about 12 m in this region. We concentrated on the experiment with assimilation over year 1, because year 1 is more anomalous than year 2.

Data assimilation performed with the objective of optimizing the initial conditions, strongly perturbs the velocity field not only initially, but for the entire following two years. The impact of assimilation on equatorial currents does not last longer than a few months. Assimilation strongly perturbs the southern cyclonic gyre. It induces an initial strong increase of the SEC, followed by a regular strong decrease which persists over the two years.

For geophysical purposes, this study shows that one year of data assimilation is not long enough to improve our knowledge of the time-invariant ocean topography in the Indian Ocean. Assimilation brings a correction over year 2, which is anticorrelated with the one over year 1. The Indian Ocean is subject to strong interannual fluctuations. If one wants to separate the oceanic signal from the geoid signal by assimilating altimetric data in oceanic models, one needs to choose at least a 4-year period.

For oceanic purposes, the improvement gained by assimilation over one year is quite impressive. Optimizing initial conditions by assimilating sea level

variations is very efficient to provide a more realistic picture of the oceanic circulation. Part of the correction brought by data assimilation is due to error in the wind, but an important part is due to the Throughflow variations prior to our experiment. There was a strong anomaly in the Throughflow in June 1985. The initial conditions for the assimilation experiments over year 1 (November 15, 1986) have been simulated by the model with closed boundary conditions. Simulations in November 1986 suffer from the lack of anomalous boundary conditions in 1985. Past the initial conditions, simulations start suffering from the lack of communication with the Pacific. The throughflow in December 1986 was also anomalous. Assimilation can compensate for this deficiency to a great extent, but this improvement shrinks with time. Past 9 months, the agreement with independent observations are degraded. Past one year of assimilation, the forecasts started from assimilated conditions are worse than those started from the non-assimilated conditions. It would be interesting to run assimilation experiments where the boundary conditions are optimized.

Note that the problem of inadequate boundary conditions may also take place at the southern boundary, where the model assumes that the Indian Ocean does not exchange mass with the Atlantic nor with the Antarctic ocean. Based on our shallow-water simulations or on Geosat, mass north of 20^{Q}S is conserved over the two years. This could indicate that such exchanges do not play a role on the variations within a two year span. This may not be true in reality. We assume in the model that the variations south of 20^{Q}S are damped. Geosat is not accurate enough to measure the meridional changes over such a large scale. This question must be reexamined with more sophisticated models (e.g. McCreary et al, 1993; Anderson and Barrington, 1993) and more accurate data (e.g TOPEX/Poseidon).

Nevertheless, the messages brought by this study are the following:

* It is possible to improve the time-invariant component of the ocean dynamic topography by assimilating sea level variations observed with an altimeter.

* The agreement between the simulated topography and the one observed by XBT is improved when altimetric data have been assimilated,

* The simulated flow in the upper layer is in agreement with other simulations, or climatologic observations. The impact of assimilation on the flow field south of the equator and north of 20°S is a mean bias or a long-term trend over two years.

* The impact was particular] y strong during year 1 as year 1987 was strongly anomalous (Perigaud and Delecluse, 1993). The anomaly in the Indian Ocean in 1987 is linked to El Nino events in the Pacific (Tourre and White, 1995).

* If one wants to simulate realistic large-scale low-frequency changes of the Indian Ocean north of 20%, one must assume realistic open boundary conditions with the Pacific ocean .

ACKNOWLEDGMENTS

The authors thank Pr J. O'Brien (FSU, Tallahassee) and ECMWF for providing wind fields over 1985-1989. They thank Dr Fieux and A. Kartavtseff (LODYC), J. R. Donguy with the staff at the TOGA Center of Brest (IFREMER), who all participated in the comparison with hydrographic data. 'l'hey thank Dr N. Smith (BRMC) for providing his analysis of XBT data. They thank Dr. M. Crepon (LODYC) and Dr P. Dandin (CNRM) for their fruitful comments on the manuscript. The authors acknowledge the use of the Ames Cray 2 to perform the model calculations. The research described in this paper was carried out by E. Greiner at LODYC, under contract DRET 91 1626/AOOO/DRET/DS/SR2 and EC MAST1 program EUROMODEL and by C. Perigaud at the Jet Propulsion Laboratory, California Institute of Technology, under contract with the National Aeronautics and Space Administration.

BIBLIOGRAPHY

Anderson, D. L. T. and D. J. Barrington, 1993: "Modeling Interannual Variability in the Indian Ocean Using Momentum Fluxes from the Operational Weather Analyses of the United Kingdom Meteorological Office and European Centre for Medium Range Weather Forecasts", J. of Geophysical Research, vol. 98, n°C7, p 12483-12499.

Cutler A.N. and J. C. Swallow, 1984: "Surface currents of the Indian Ocean (to25S, 100E)", 10S Tech. Rep. 187.

Chao Y., D. Halpern and C. Perigaud, 1993: "Sea surface height variabilities in the tropical Pacific Ocean", J. Geophys. Res., 98, 6947-695

Dombrowsky E. and De Mey P., 1992: "Continuous Assimilation in an Open Domain of the Northeast Atlantic: 1. Methodology and application to Athena-88", J. Geophys. Res., 97,9719-9731.

Fieux M., F. Schott and J. Swallow, 1986: "Deep boundary current in the western Indian Ocean, revisited", Deep-Sea Res., 415-426.

Gent P. R., K. O'Neill and M.A. Cane, 1983: "A model of the semi-annual oscillations in the equatorial Indian Ocean", J. Phys. Oceanogr., 13, 2148-2160.

Greiner E. and C. Perigaud, 1994: "Assimilation of Geosat altimetric data in a nonlinear reduced-gravity model of the Indian Ocean by adjoint approach, part 1 : methods ans statistical results", Journal of Physical Oceanography, vol 24, n°8, p1783-1804.

Kindle J.C. and J. D.Thompson, 1989: "The 26- and 50-day oscillations in the western Indian Ocean: Model results", J. Geophys. Res., 94, 4721-4736.

Kindle, J. C., G. W. Heburn, and R. C. Rhodes, 1987: "An estimate of the Pacific to Indian Ocean Throughflow from a global numerical model", A report of the U.S. TOGA Workshop on the dynamics of the equatorial oceans, Further Progress in Oceanography, Nova University Press.

Levitus, S., 1982: "Climatological atlas of the world ocean", NOAA Prof. Pap. 13, 173 pp., U.S. Dep. of Commer., Rockville, Md.

McCreary J. P., P. K. Kundu and R. L. Molinari, 1993: "A numerical investigation of dynamics, thermodynamics and mixed-layer processes in the Indian Ocean", Prog. Oceanogr., vol. 31, pl 81-244.

Meyers G., R. Bailey and T. Worby, 1994a: "Volume transport of Indonesian Throughflow", Deep-Sea Res. (in press).

Meyers G., T. Qu and J.K. Donguy, 1994b: "Ocean mechanisms of SST variability in the South tropical Indian Ocean", 518-524. Proceedings of the Internal Conf. on Monsoon variability and prediction, trieste, WCRP-84, WMO/TD 69, case Postale 2300, CH-I211, Geneva, 20 Switzerland.

Molinari R. L., D.B. Olson and G. reverdin, 1990: "Surface current distirbution in the tropical Indian Oceanderived from compilation of surface buoy trajectories", J. Geophys. res., 95, 7217-7238.

Perigaud and Delecluse, 1992: "Annual sea level variations in the tropical Indian Ocean", J. Geophys. Res., 97,20169-20178.

Perigaud C. and Delecluse P., 1993 : "Interannual sea level variations in the tropical Indian Ocean from Geosat and shallow-water simulations", Jour. Phys Oceanog., 23, 1916-1934.

Potemra J.T., M. Luther, and J.J. O'Brien, 1991: "The seasonnal circulation of the upper ocean in the Bay of Bengal", J. Geophys. Res., 96, 12667-12684.

Rao R. R., R.L. Molinari and J.F. Festa, 1989: "Evolution of the climatological mean surface thermal structure of the tropical Indian Ocean. 1. Description of mean monthly mixed layer depth, sea surface temperature, surface current and surface meteorological fields", J. Geophys. Res., 94, 10801-10815.

Rebert, J. P., 1993: "Data quality control at the TOGA subsurface data Centre", Manual of quality control procedures for validation of Oceanographic data, Manual and guides 26, UNESCO.", J. Geophys Res., 93,4963-4974.

Roemmich D. and C. Wunsch, 1982: “On combining satellite altimetry with hydrographic data”, J. Mar. Res., 40, 605-619.

Schott F., 1992: “Flows connections with the southern hemisphere and Bay of Bengal”, WOCE Report 96/92, WOCE International Project Office, Wormley, Appendix 5.

Schott F., M. Fieux, J. Kindle, J.C. Swallow and R. Zantopp, 1988: “The boundary currents east and north of Madagascar, 2 Direct Measurements and model comparisons”, J. Geophys Res., 93,4963-4974.

Schott F., J.C. Swallow and M. Fieux, 1990: “the Somali current at the equator: annual cycle of currents and transports in the upper 1000m and connection to neighboring latitudes”, Deep-Sea Res., 37, 1825-1848.

Schott F., J. Reppin, D. Quadfasel, and J. Fisher, 1995: “Currents and transports of the Monsson Current south of Sri Lanka:, J. Geophys. Res.

Smith N. R., J.E. Blomley and G. Meyers, 1991: “A univariate statistical interpolation scheme for subsurface thermal analyses in the tropical oceans.”, Progr, Oceanography, 28, 219-256.

Smith N. R., 1995: “An improved system for tropical ocean sub-surface temperature analyses”, J. Atmos. Oceanic. Technol., to appear.

Swallow J., M. Fieux and F. Schott, 1988: “The boundary Currents East and North of Madagascar. 1. geostrophic Currents and transports”, J. Geophys. Res., 93,4951-4962.

Tourre, Y., and W. White, 1995: EN SO signals in global upper ocean thermal structures. J. Phys. Oceanog., in press.

Woodberry K., Luther M. and J. O’Brien, 1989: "The wind-driven seasonal circulation in the southern tropical Indian ocean”, J. Geophys. Res., 94, 17985-18002.

Wyrtki K., 1973: “An equatorial jet in the Indian Oceanm". Science, 181, 262-264.

Table 1: Comparison along the XBT section between D20 and model simulations without assimilation (NOAS), with ASS1 or ASS2 experiment . Values are the spatial correlation and the rms difference at a given month.

Month	Correlation			RMS Diff (m)		
	NOAS	Assl	ASS2	NOAS	ASS1	ASS2
Nov	0.71	0.91	0.93	22	18	15
Jan	0.83	0.88	0.93	26	17	13
Mar	0.82	0.89	0.95	25	15	12
May	0.85	0.87	0.92	22	18	16
Jul	0.82	0.87	0.92	22	18	16
Sep	0.66	0.44	0.49	19	24	23

Table 2: Comparison North of 20?3 between D20 and model simulations without assimilation (NOAS), with ASS1 or ASS2 experiment . Values are the spatial correlation and the rrns difference for the surfaces computed on (1) November 1986 or (2) averaged over the first 6 months.

	Correlation			RMS Diff (m)		
	NOAS	ASS1	ASS2	NOAS	ASS1	ASS2
(1)	0.53	0.61	0.68	28	28	24
(2)	0.69	0.73	0.80	19	20	15

Figure list

Figure 1: Mean dynamic topography (in cm) over year 1 for the model without assimilation (top) and with ASS2 assimilation (bottom). Location of the XBT data studied in section 2 is indicated by (*).

Figure 2: Surface dynamic height (in cm) relative to 150m (plain) or simulated sea level along the XBT line. Only one arbitrary constant was retrieved from all plots (see text). The dotted line is for the model without assimilation, the dashed line is for ASS 1, the dot-dashed curve is for ASS2. Signals are plotted for January 1987, March 1987, May 1987 and August 1987.

Figure 3: Thermocline depth (in m) along the XBT line. The plain line is for the 20ºC isotherm depth, the dotted line for the model without assimilation, the dashed line is for ASS 1, the dot-dashed curve is for ASS2.

Figure 4: Thermocline depth (in m) simulated without assimilation difference to D20 (top) or to the model with assimilation (bottom).Time is November 15, 1986.

Figure 5: Mean dynamic topography (in cm) over year 2 for the model without assimilation (top) and for ASS2 (bottom) (same as Figure 1, but for year 2).

Figure 6: Yearly-averaged difference of dynamic topography (in cm) between year 1 and year 2. Signals are derived from the model without assimilation (top) and from the model with ASS2 (bottom). The ASS2 experiments were performed on each year separately .

Figure 7: Optimal correction (in cm) of the yearly-averaged dynamic topography obtained with ASS2 for year 1 (top) and for year 2 (bottom) .

Figure 8: Zonally averaged thermocline depth (in m) as a function of latitude. The two plots correspond to the yearly averaged depth after spin-up by FSU

wind (plain) or ECMWF wind (dotted).

Figure 9: Yearly averaged difference (in cm) of dynamic topography between FSU and ECMWF simulations. Signals are for year 1 (top) and for year 2 (bottom).

Figure 10: Difference between the yearly averaged and the 1985-1988 averaged dynamic topography (in cm) for year 1 (top) and year 2 (bottom). Results are derived from the 20ºC isotherm depth.

Figure 11: Transport (in Sverdrup) across 110ºE between 10°S and 20°S. Positive is for eastward transport. Plain thick line is the model simulations without assimilation driven by FSU winds over 1985-1988. Dashed and dotted lines correspond to the climatologic run after spin-up driven by FSU monthly winds averaged over 1985-1988. Dashed is the geostrophic transport, dotted is the full simulated transport. The thin line is the transport variations derived by applying geostrophy on Geosat sea level variations.

Figure 12: Initial velocity fields (in cm/s) simulated by the model without assimilation (left) and with ASS 1 (right).

Figure 13: Transport (in Sverdrup) across different sections simulated by the model without assimilation (dotted line) and with ASS 1 (plain line) as a function of time between November 25, 1986 and November 15, 1988.

SECTION 13a	90°E-9°S	90°E-20°S	Positive to the East
SECTION 13b	75°E-9°S	75°E-20°S	Positive to the East
SECTION 13c	49°E-100S	49°E-12°S	Positive to the East
SECTION 13d	50°E-2°S	50°E-8°S	Positive to the East
SECTION 13e	40°E-0°N	60°E-0°N	Positive to the North
SECTION 13f	41 “E-12°S	48”E-12°S	Positive to the North
SECTION 13g	510E-90N	52°E-8°N	Positive to the North-East
SECTION 13h	78°E-0°N	78°E-3°N	Positive to the East

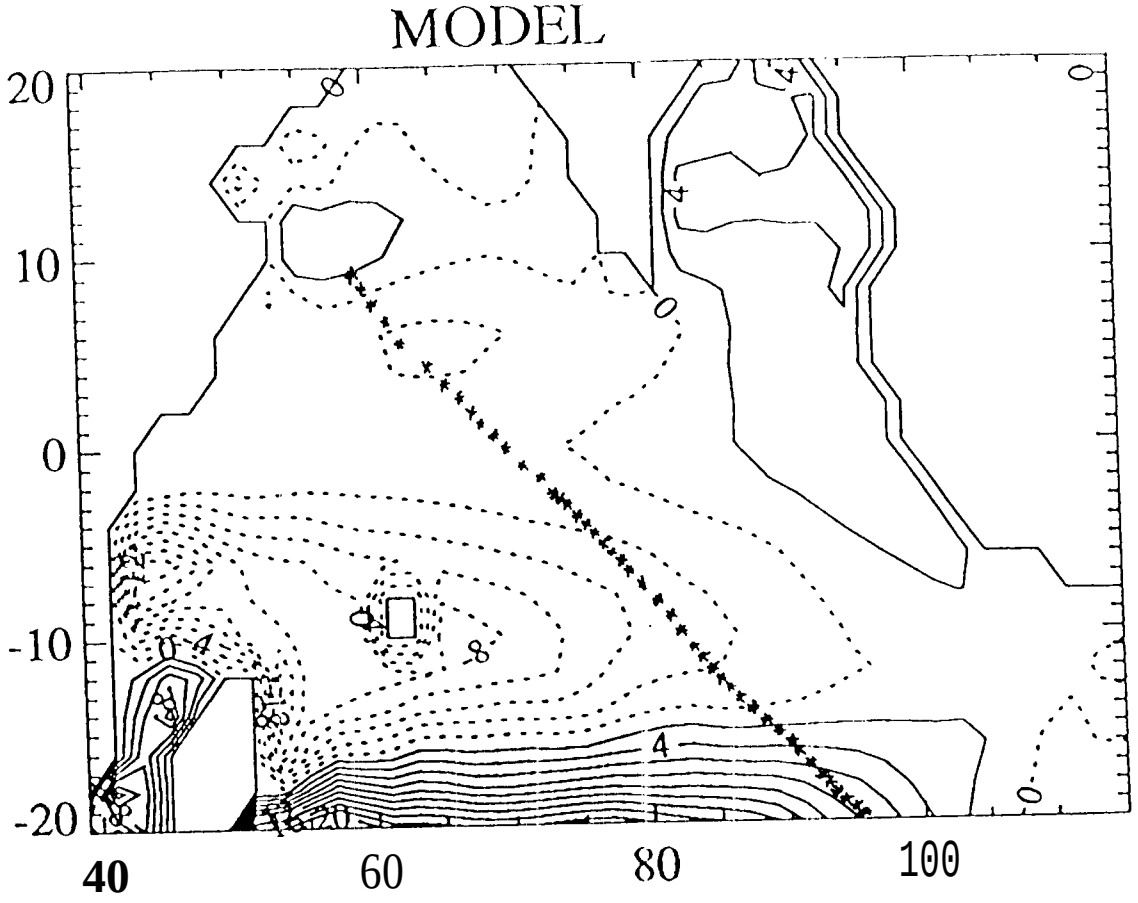

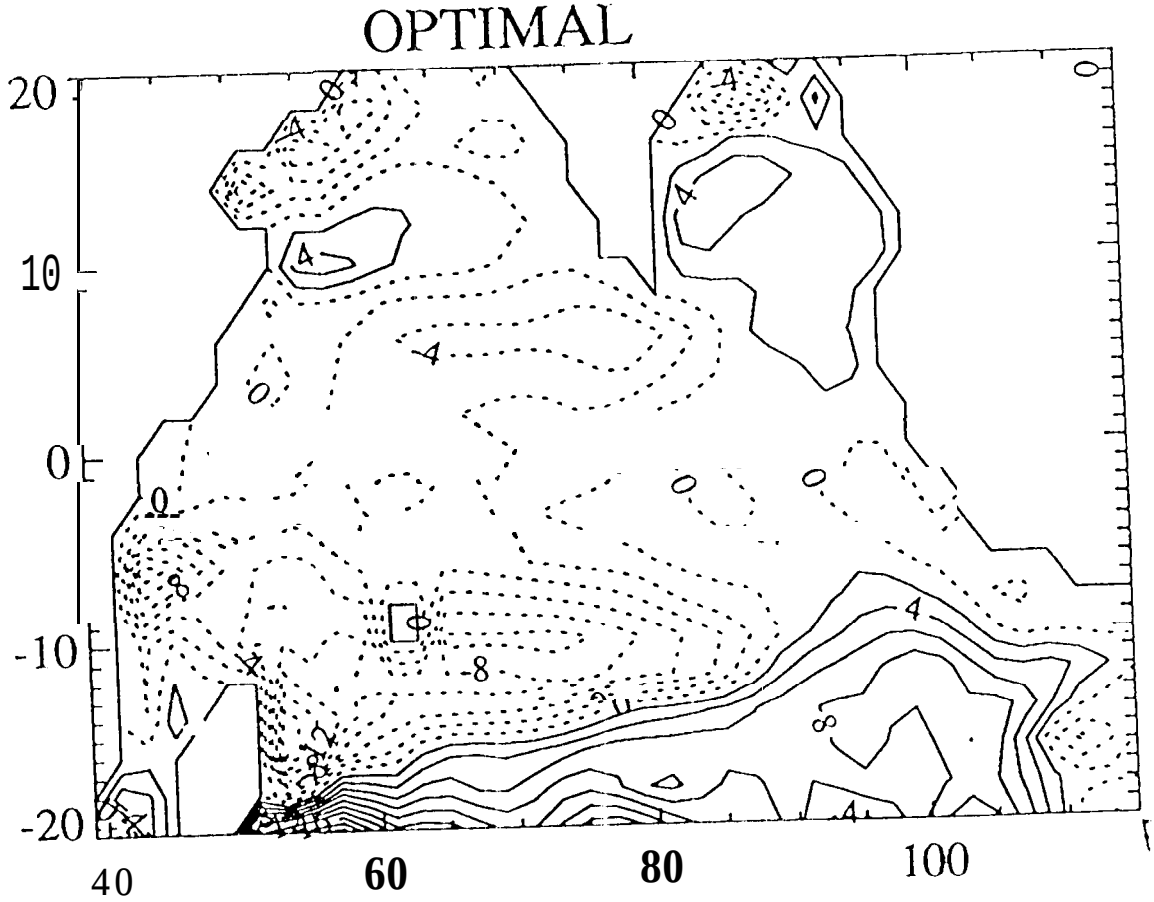

Figure 1

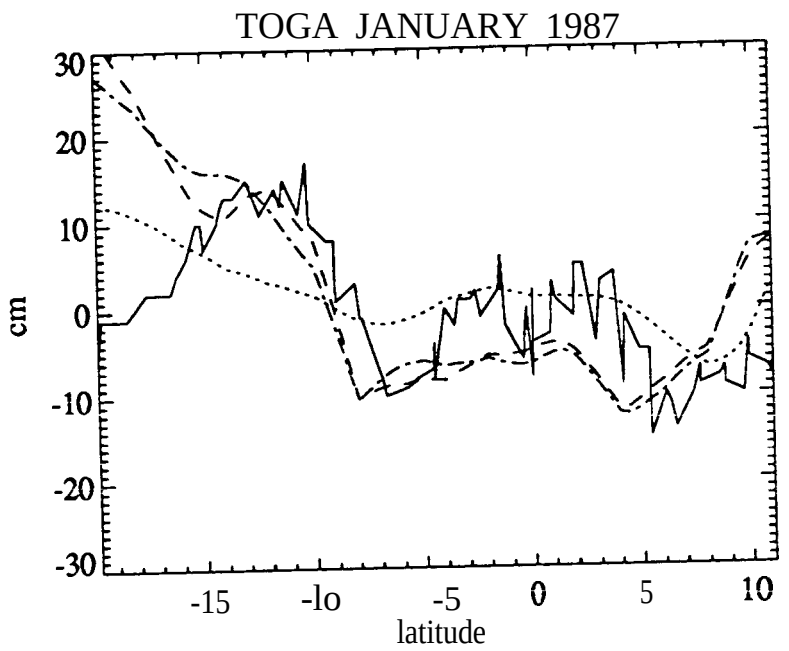
TOGA JANUARY 1987
cm
30
20
10
0
-10
-20
-30
-15
-lo
-5
0
5
10
latitude

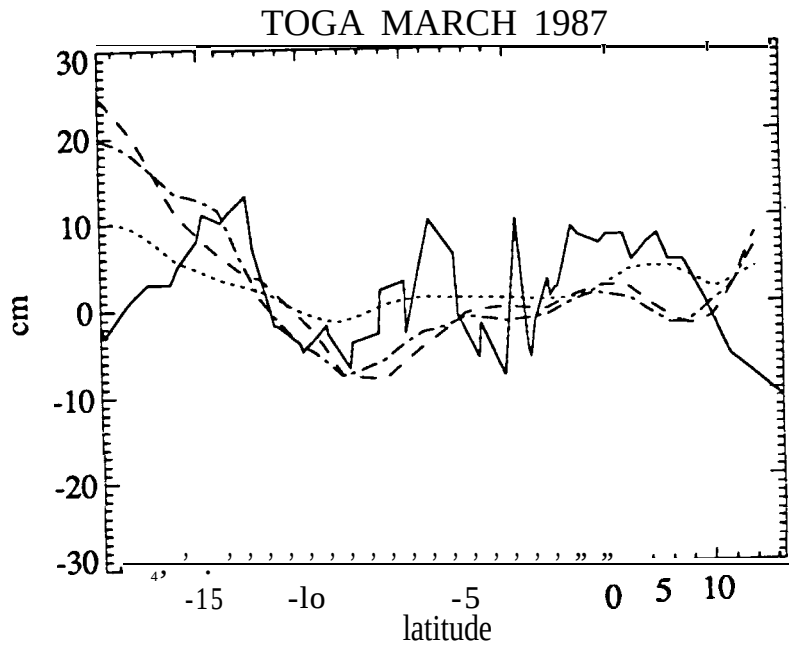
TOGA MARCH 1987
cm
30
20
10
0
-10
-20
-30
-15
-lo
-5
0
5
10
latitude

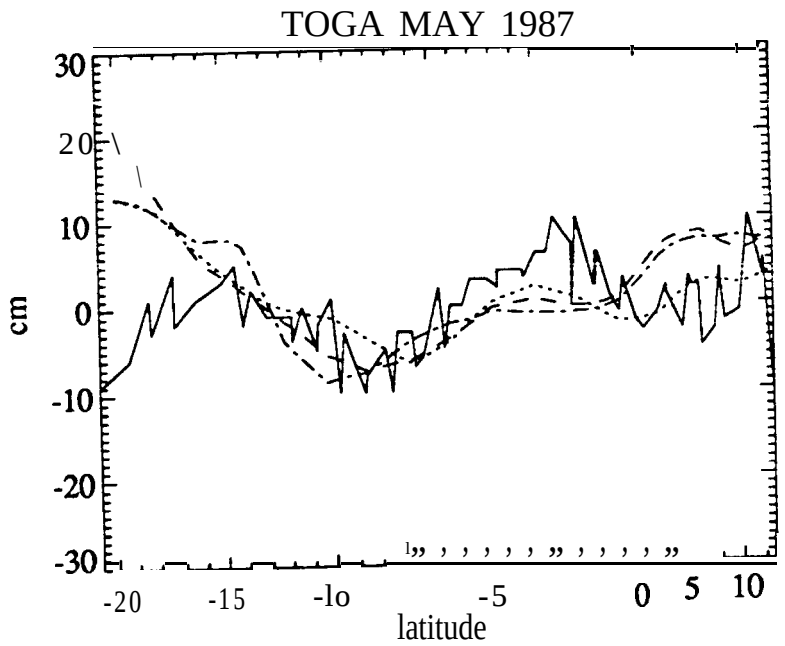
TOGA MAY 1987
cm
30
20
10
0
-10
-20
-30
-20
-15
-lo
-5
0
5
10
latitude

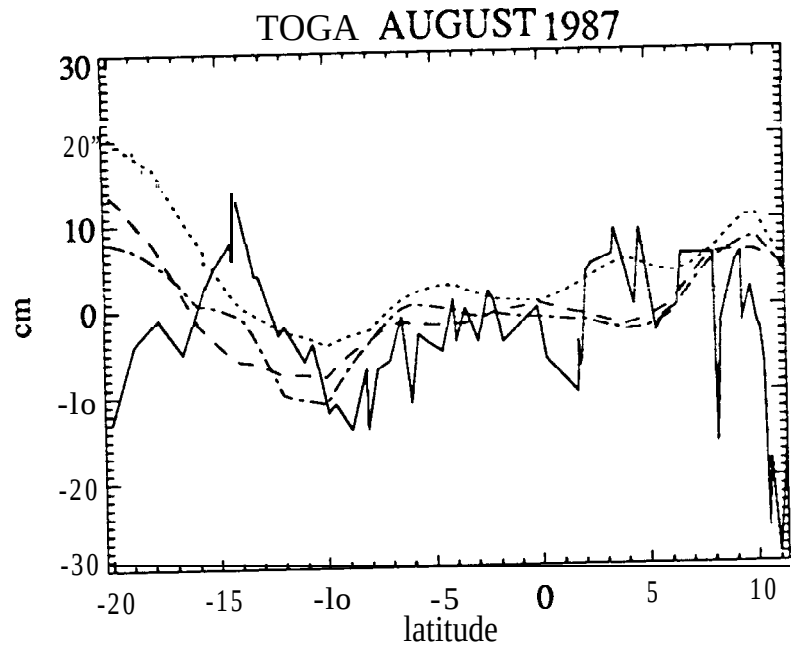
TOGA AUGUST 1987
cm
30
20
10
0
-lo
-20
-30
-20
-15
-lo
-5
0
5
10
latitude

June 2

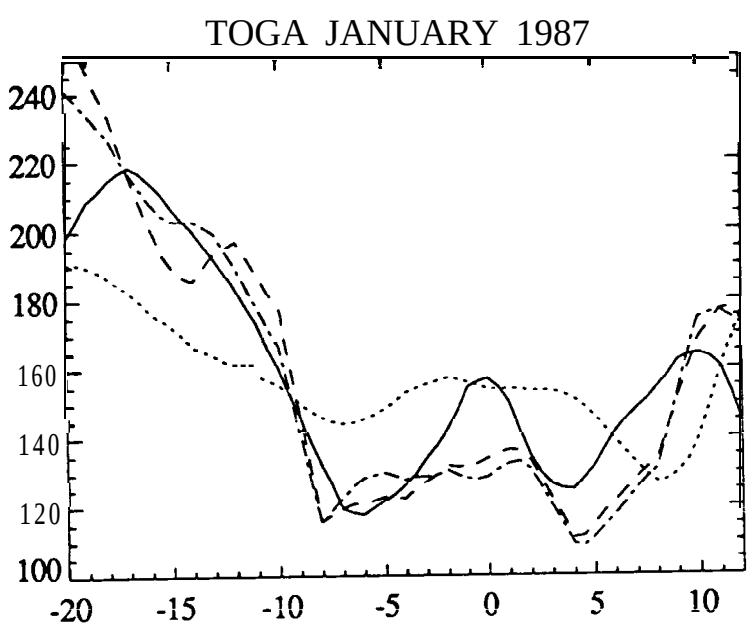
TOGA JANUARY 1987
240
220
200
180
160
140
120
100
-20
-15
-10
-5
0
5
10

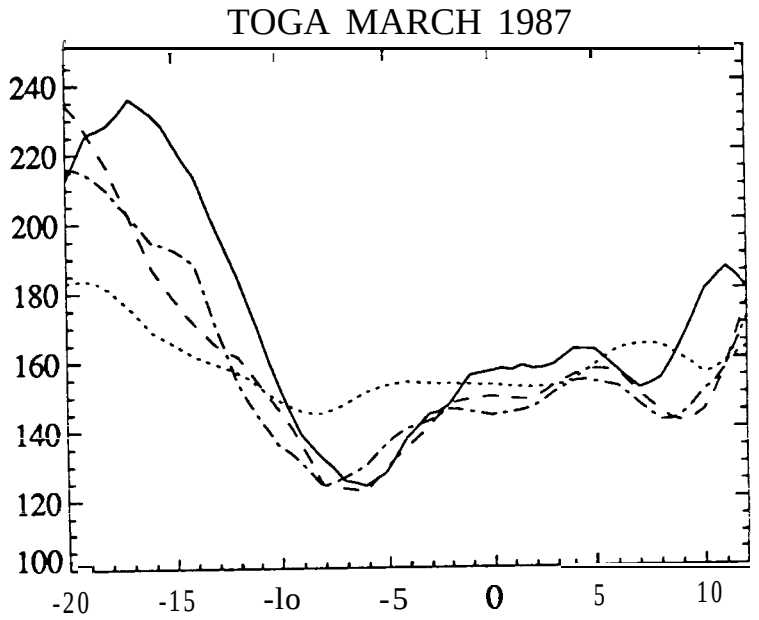
TOGA MARCH 1987
240
220
200
180
160
140
120
100
-20
-15
-lo
-5
0
5
10

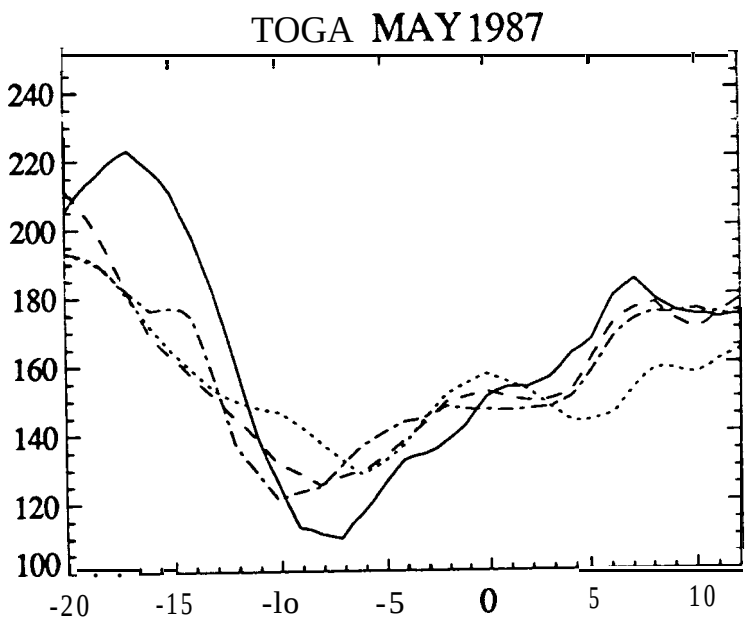
TOGA MAY 1987
240
220
200
180
160
140
120
100
-20
-15
-lo
-5
0
5
10

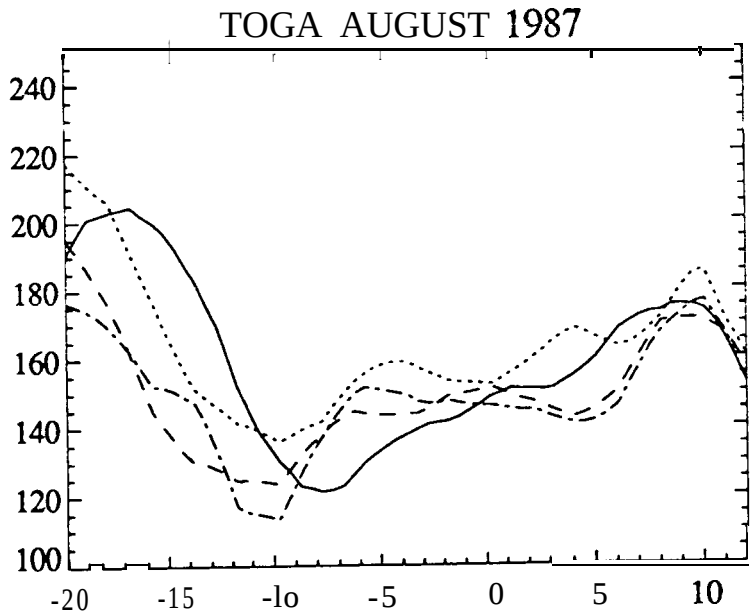
TOGA AUGUST 1987
240
220
200
180
160
140
120
100
-20
-15
-lo
-5
0
5
10

Figure 2

MODEL WITHOUT ASSIM - D20

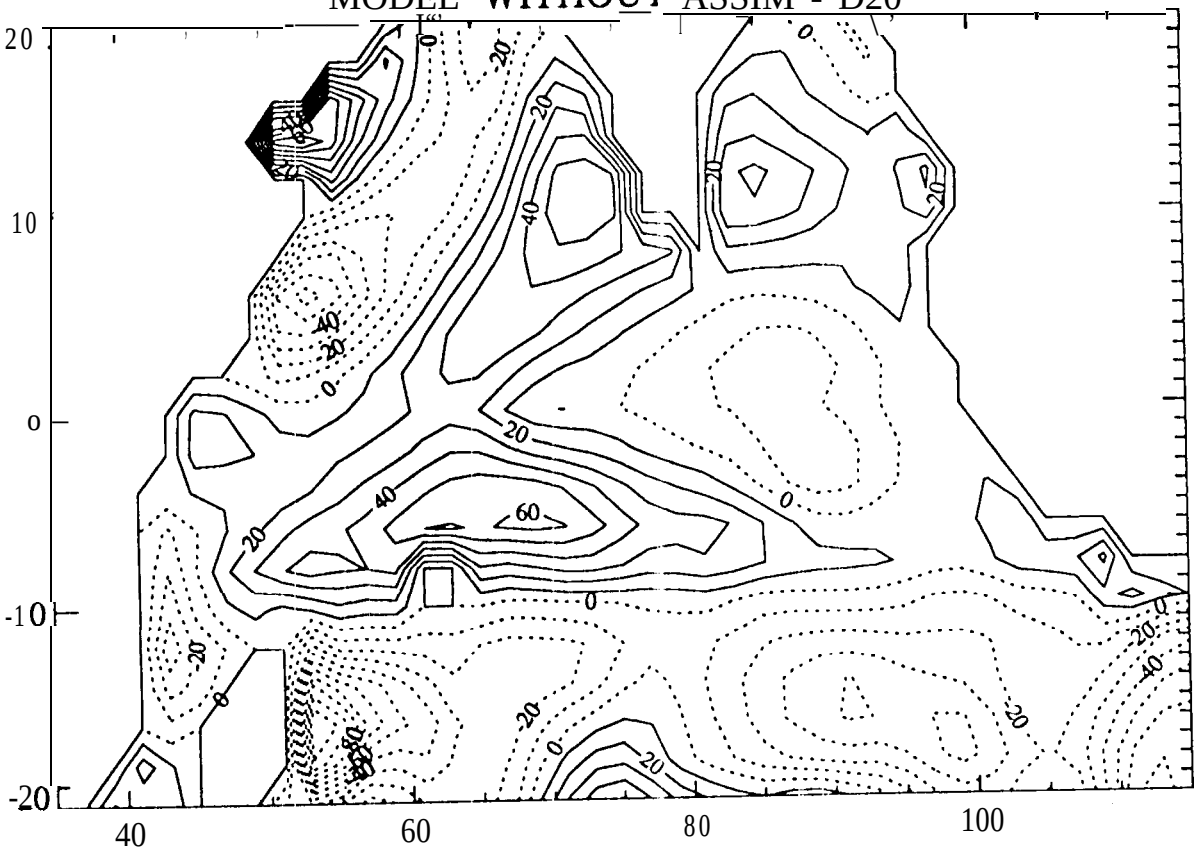

MODEL WITHOUT ASSIM - MODEL WITH ASS 1

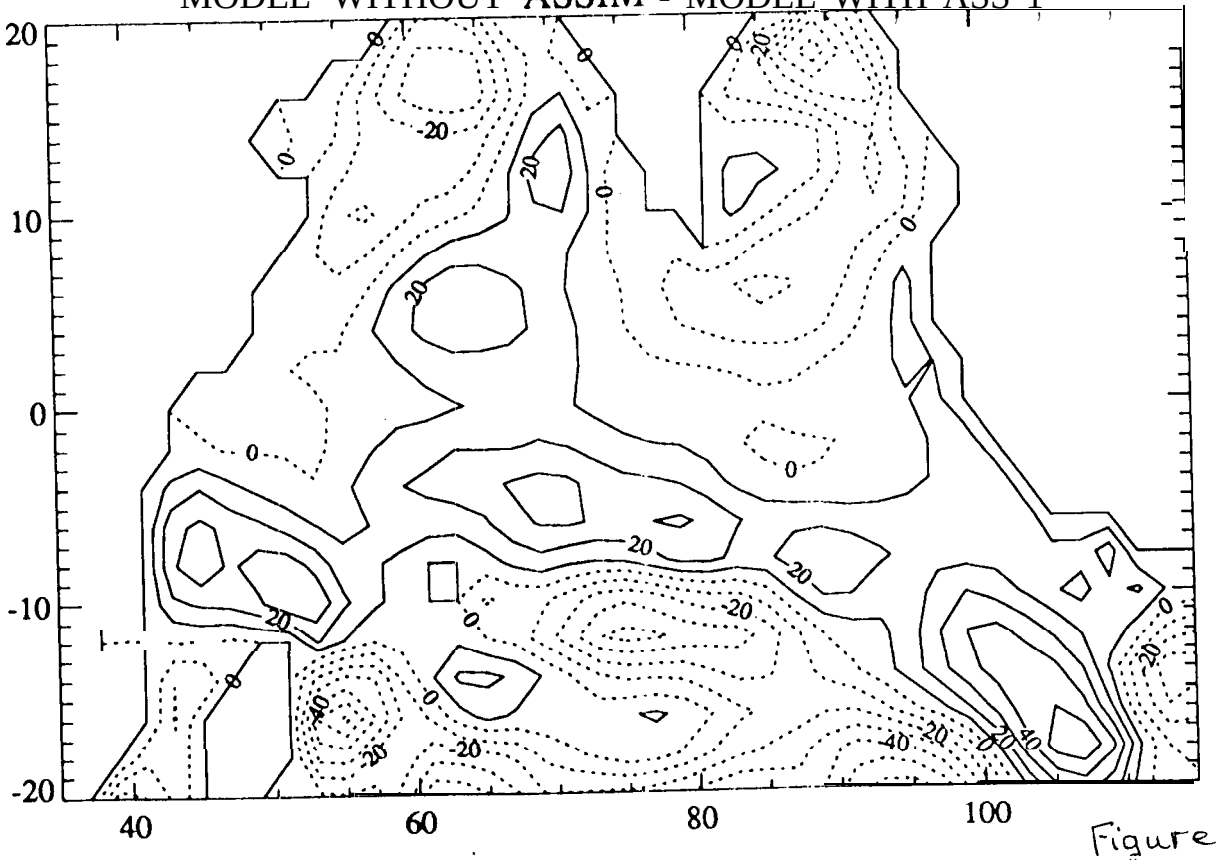

Figure 4

MEAN DYNAMIC TOPOGRAPHY YEAR 2 (cm)

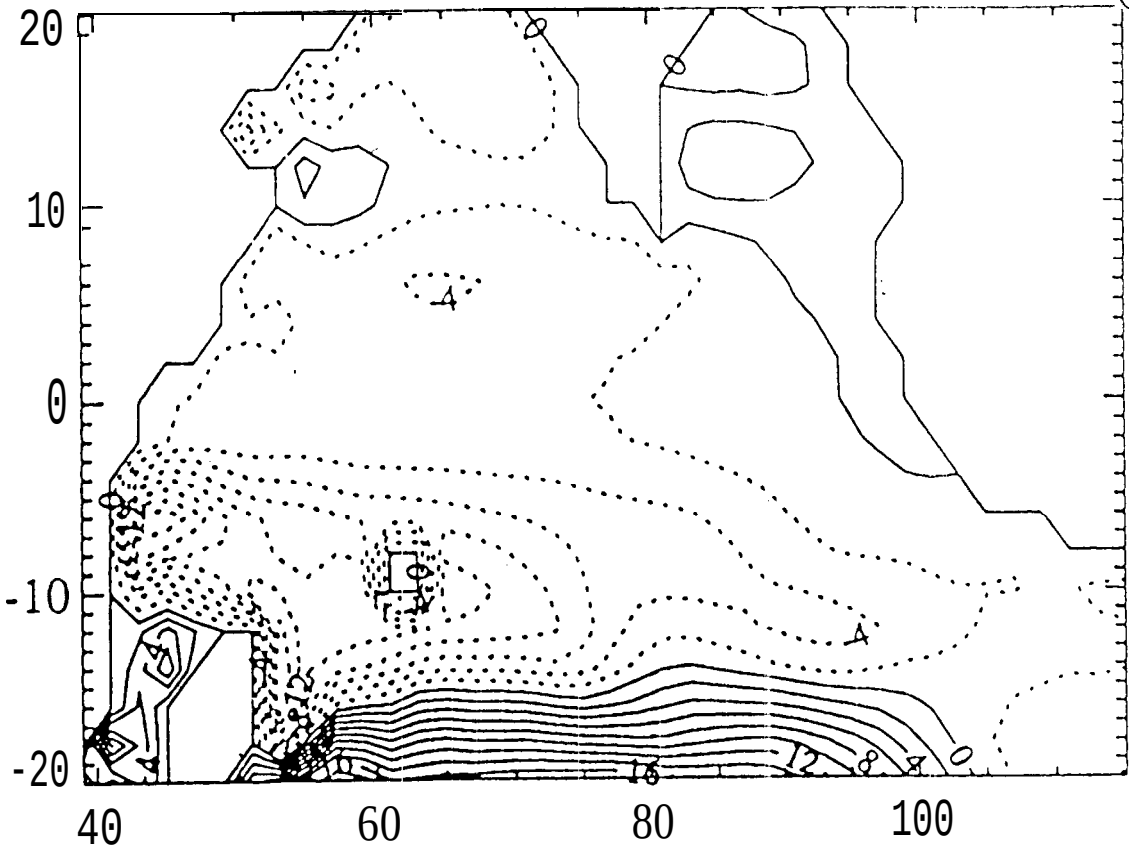

OPTIMAL YEAR 2

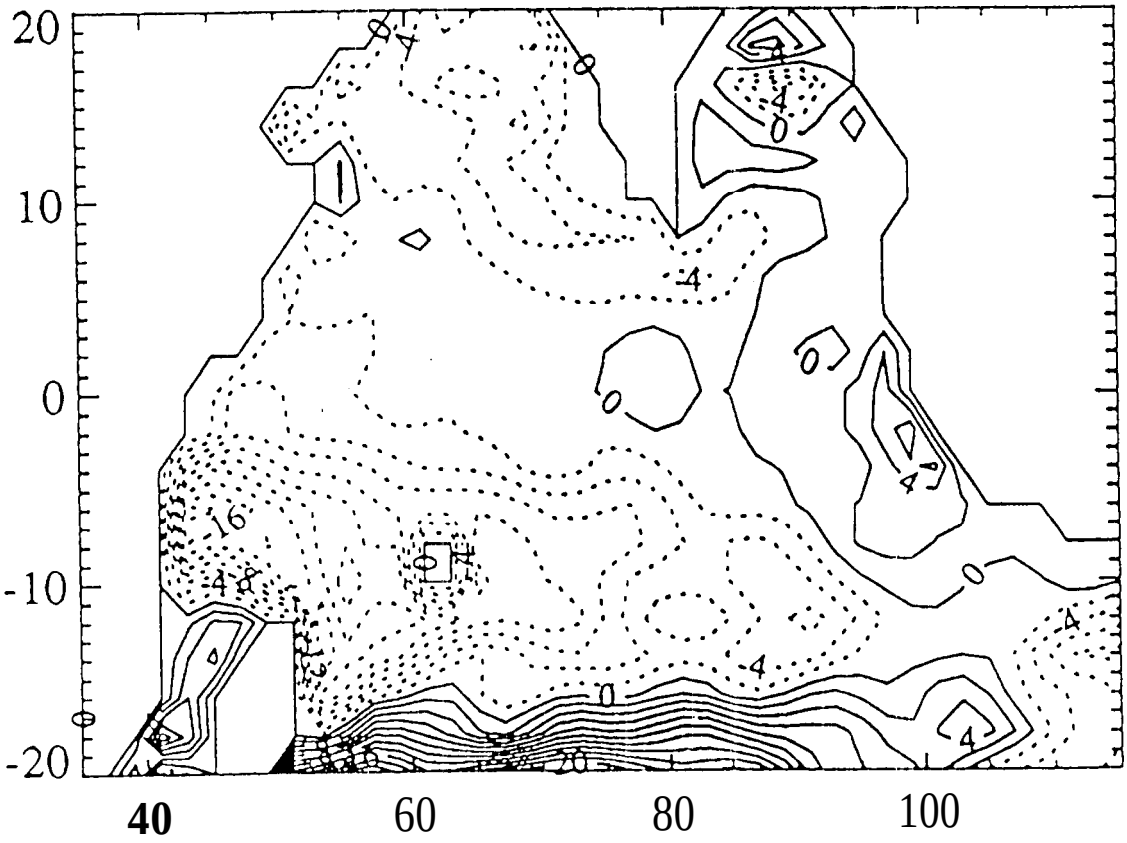

MEAN YEAR 1- YEAR 2

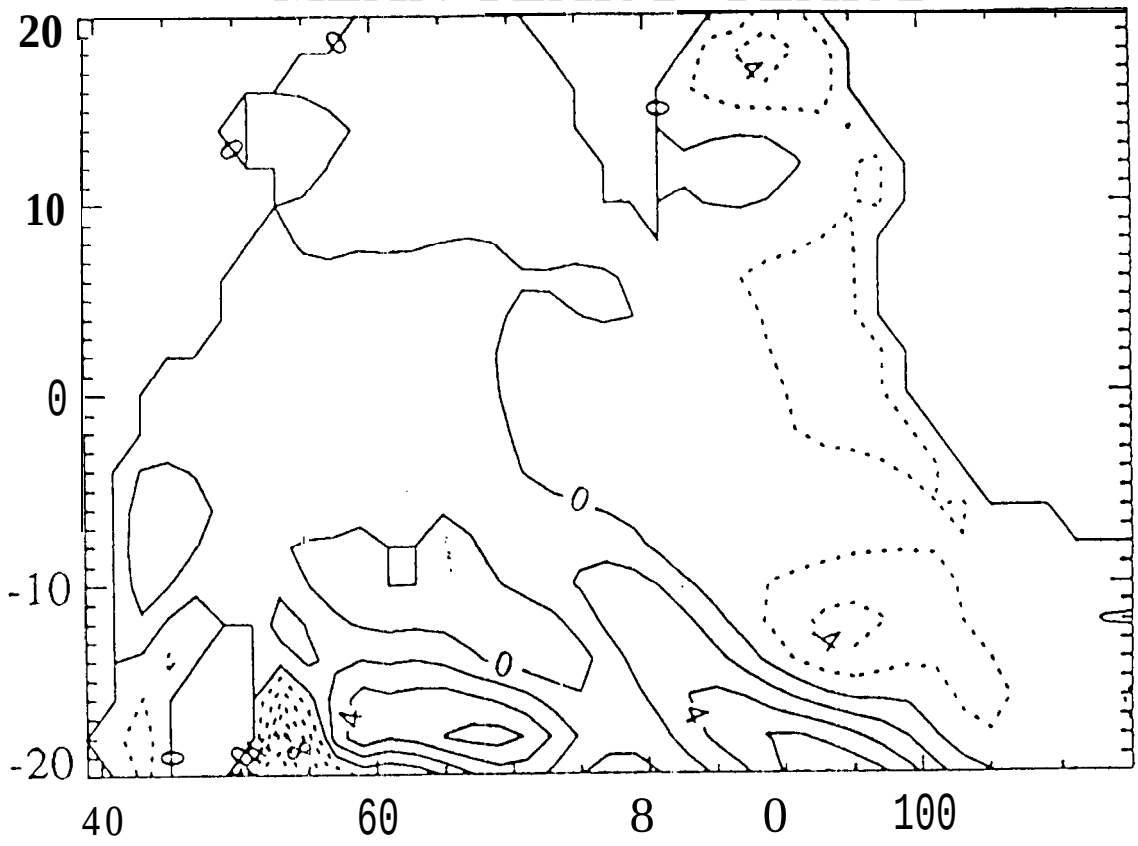

MODEL WITH ASSIMILATION

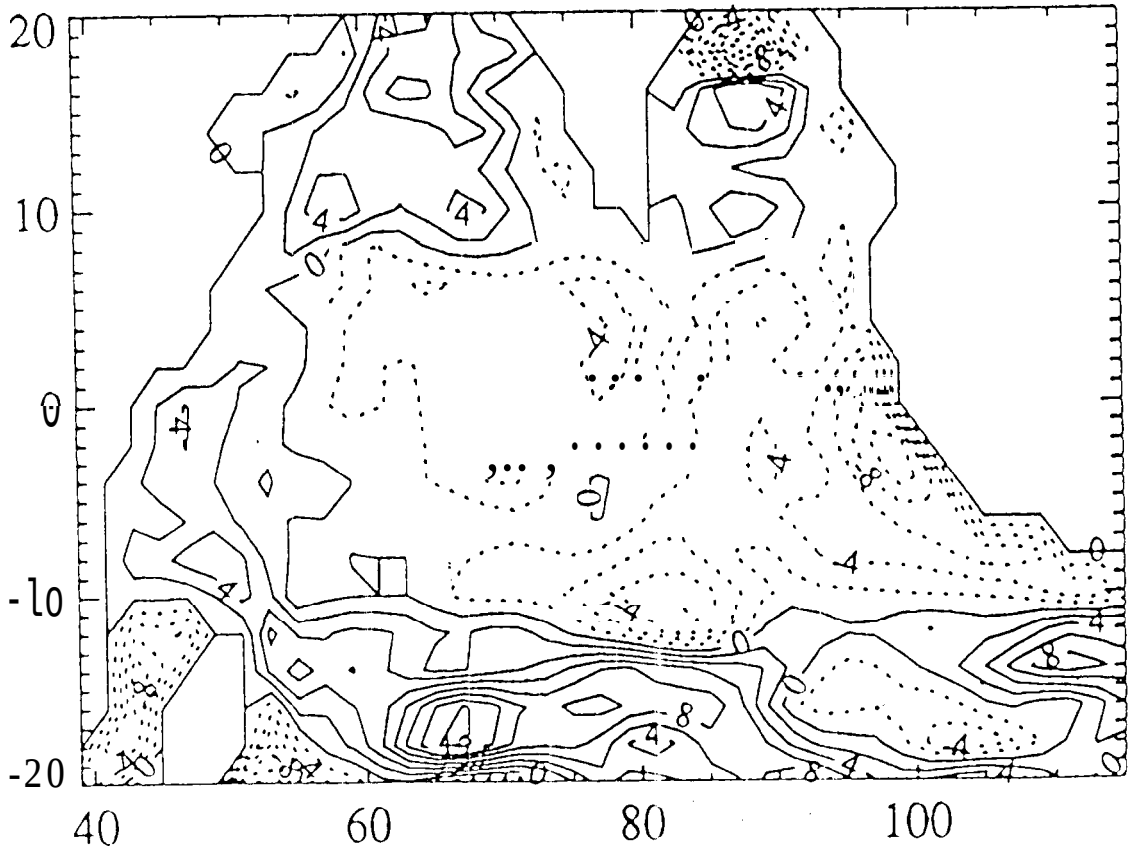

Fig 6

ASS2 OVER YEAR 1 and ASS2 OVER YEAR 2

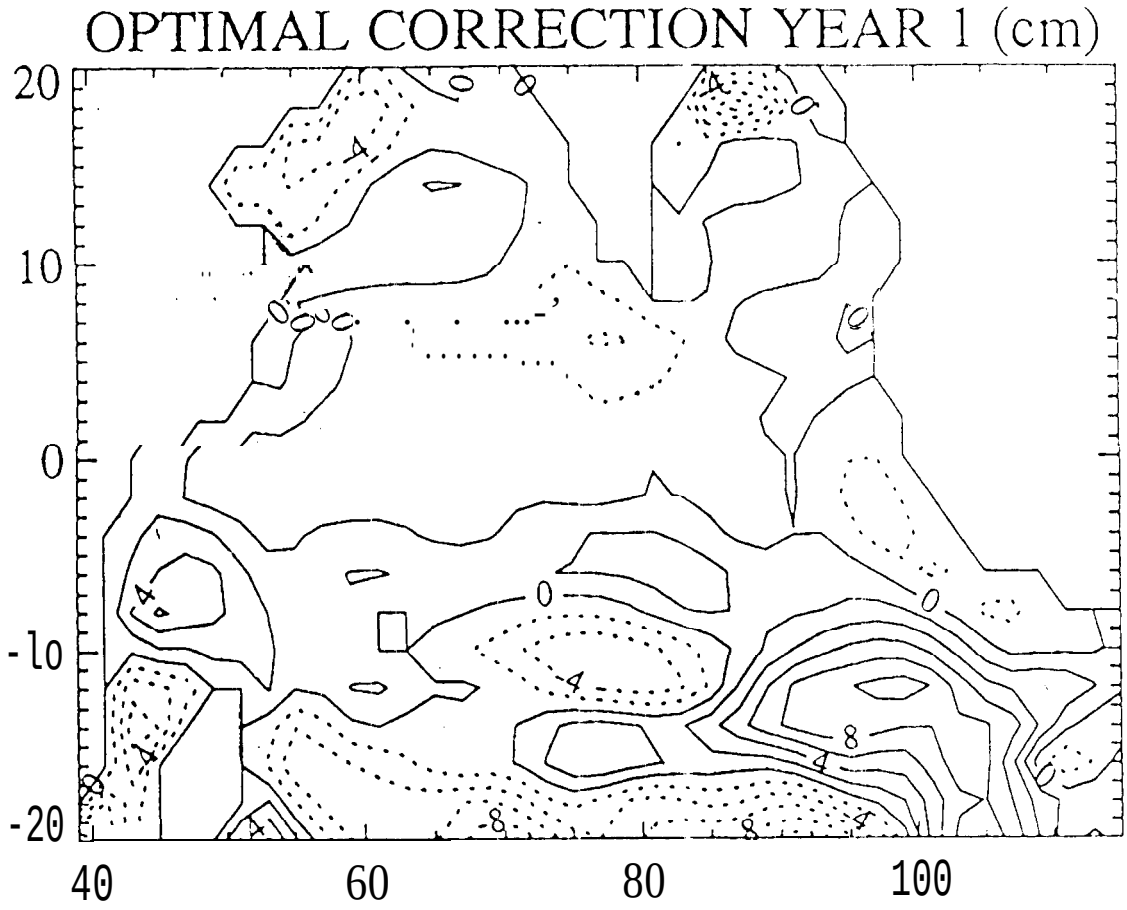

relative to mean year 1

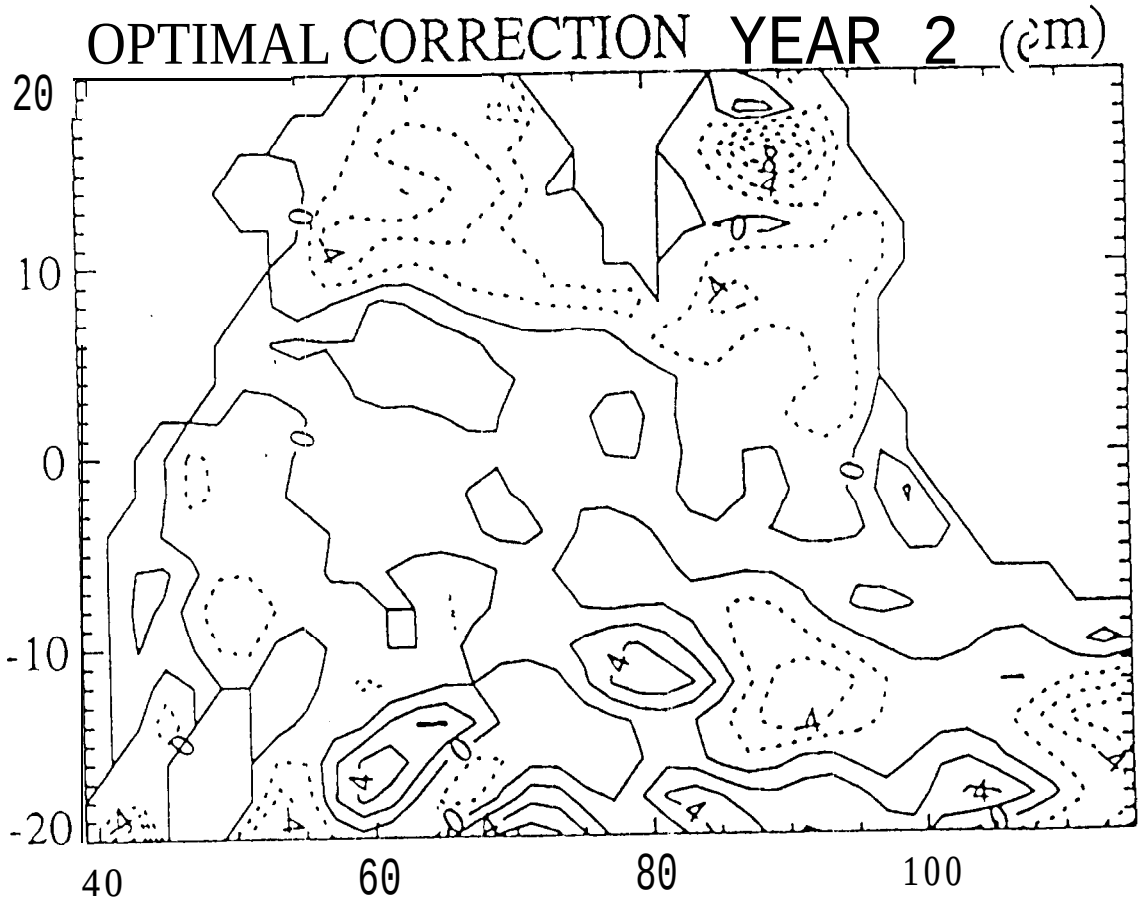

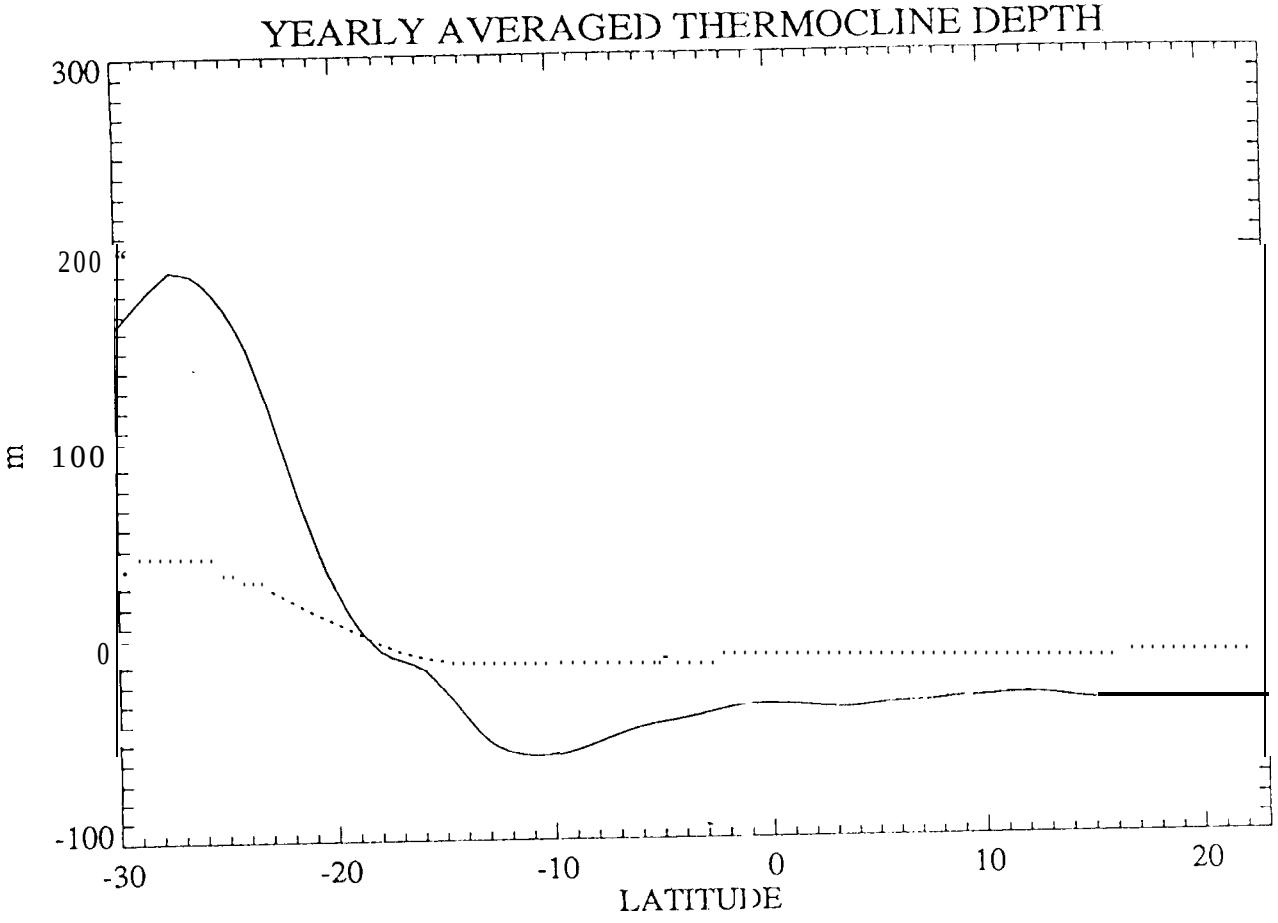
YEARLY AVERAGED THERMOCLINE DEPTH
300
200
100
0
-100
m
-30
-20
-10
0
10
20
LATITUDE

MODEL FSU- ECMWF YEAR 1

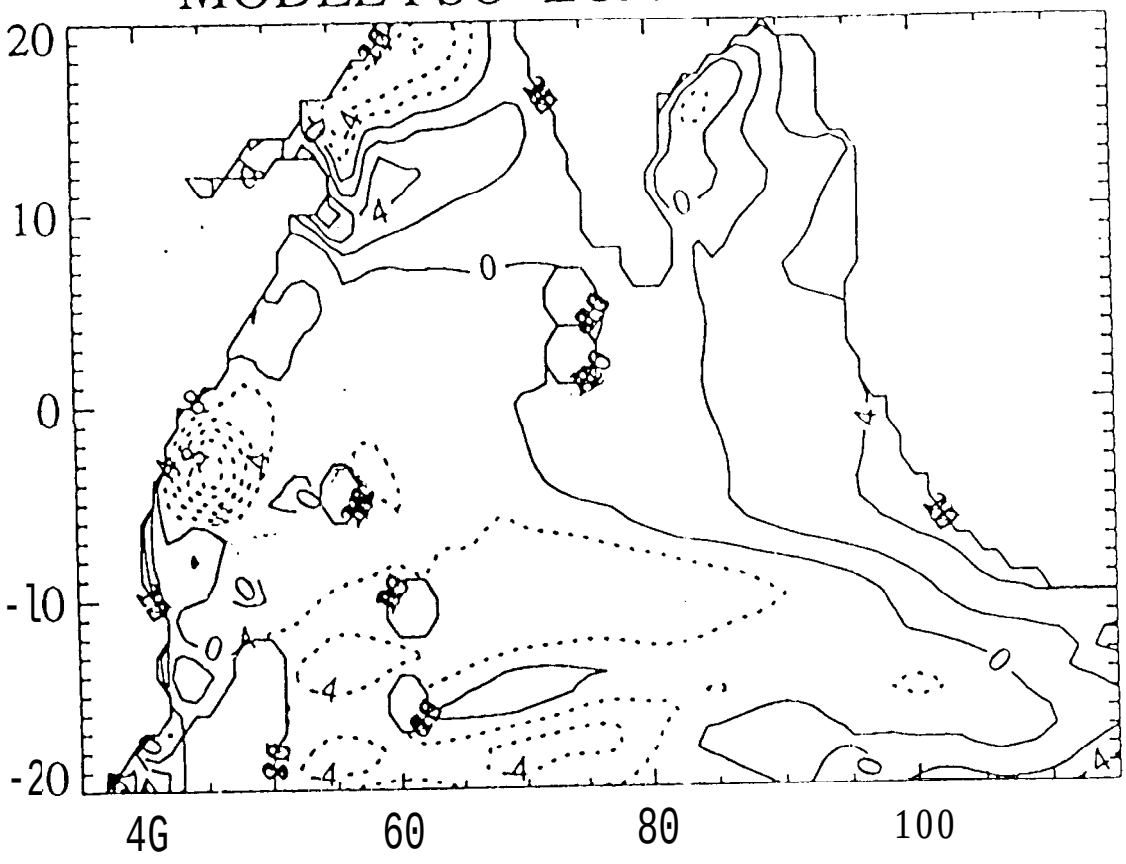

MODEL FSU - ECMWF YEAR 2

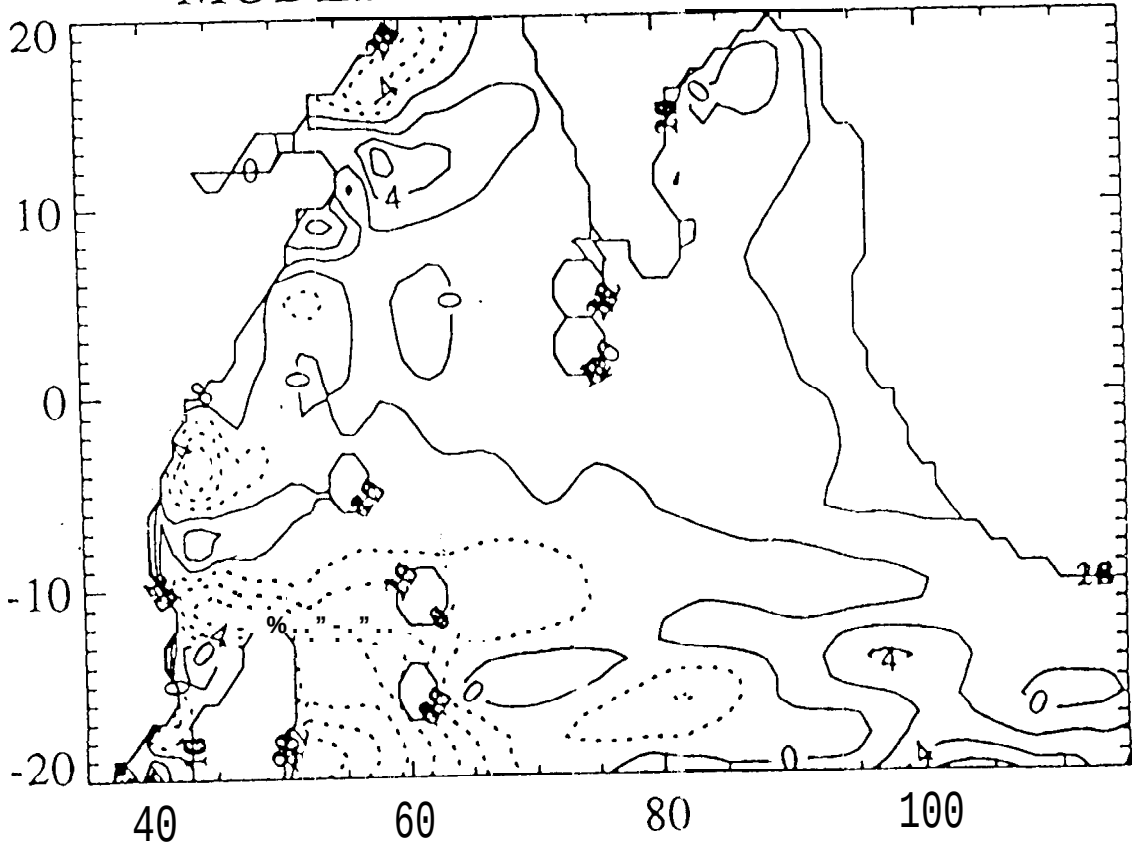

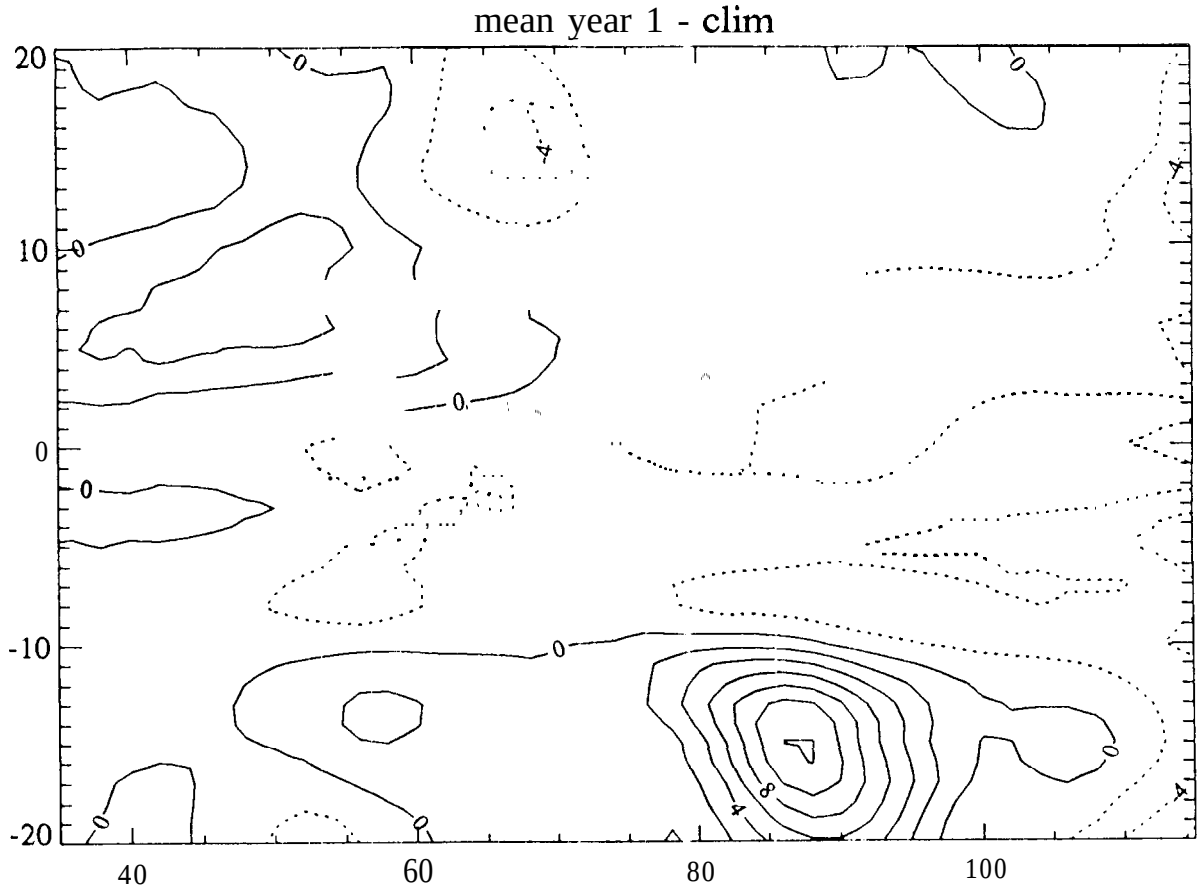
mean year 1 - clim
20
10
0
-10
-20
40
60
80
100

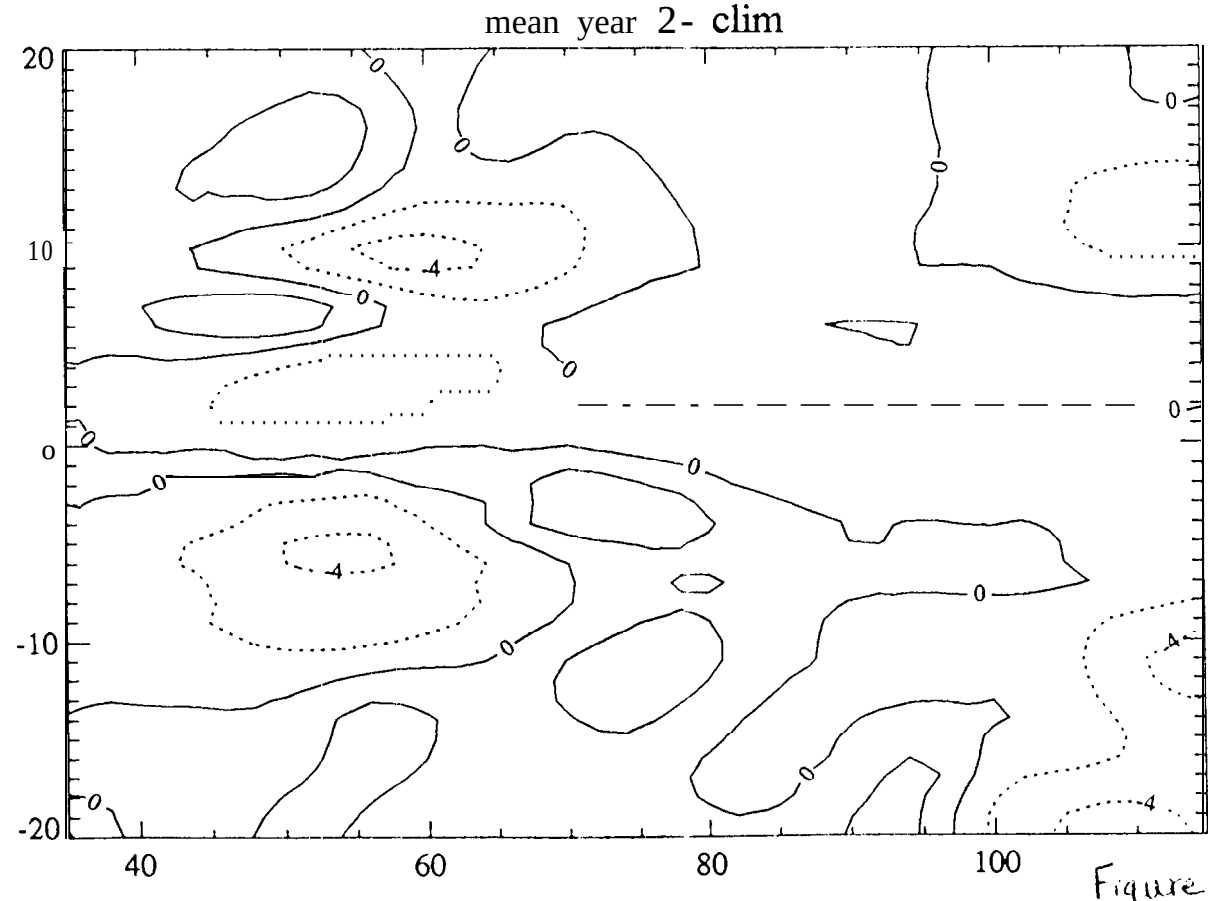
mean year 2- clim
20
10
0
-10
-20
40
60
80
100

Figure 10

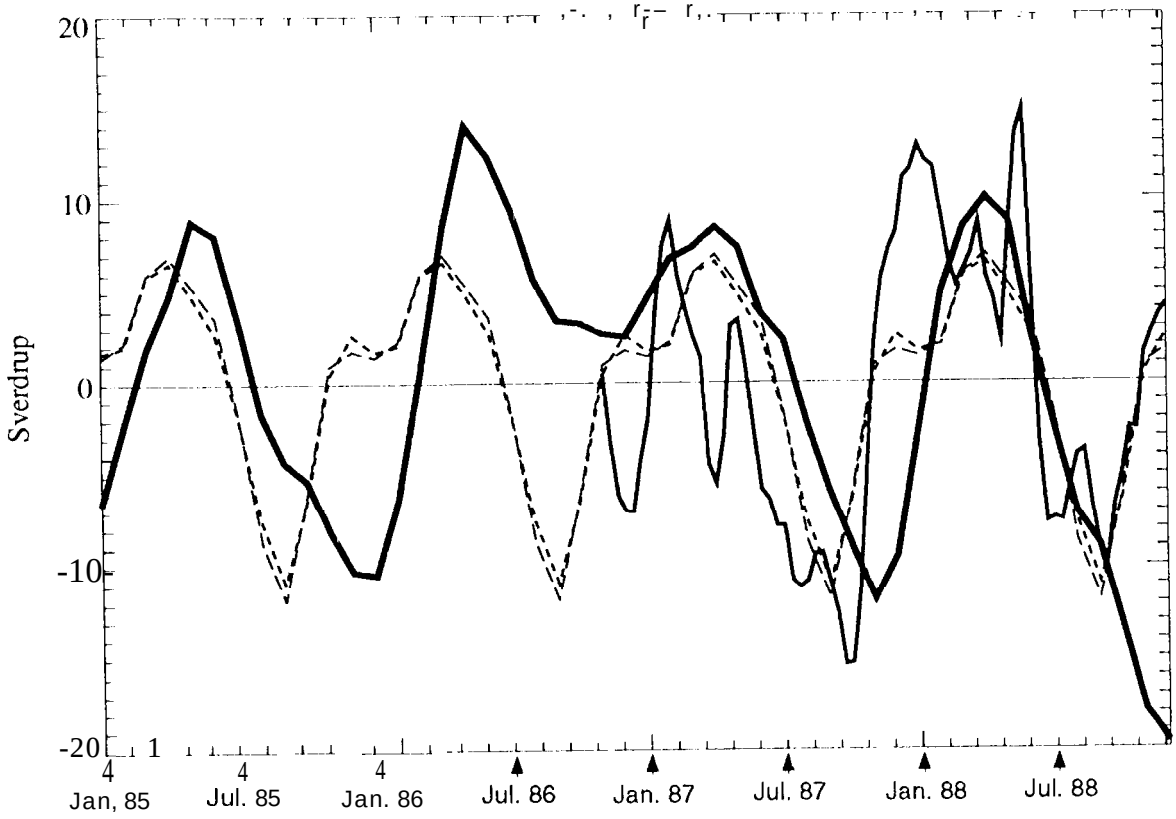
20
10
0
-10
-20
Sverdrup
Jan, 85
Jul. 85
Jan. 86
Jul. 86
Jan. 87
Jul. 87
Jan. 88
Jul. 88

Figure 11

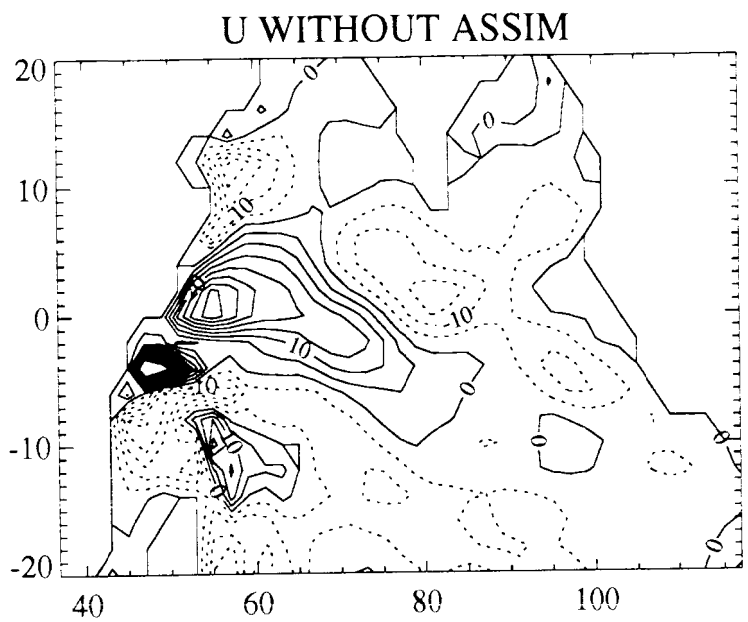
U WITHOUT ASSIM
20
10
0
-10
-20
40
60
80
100

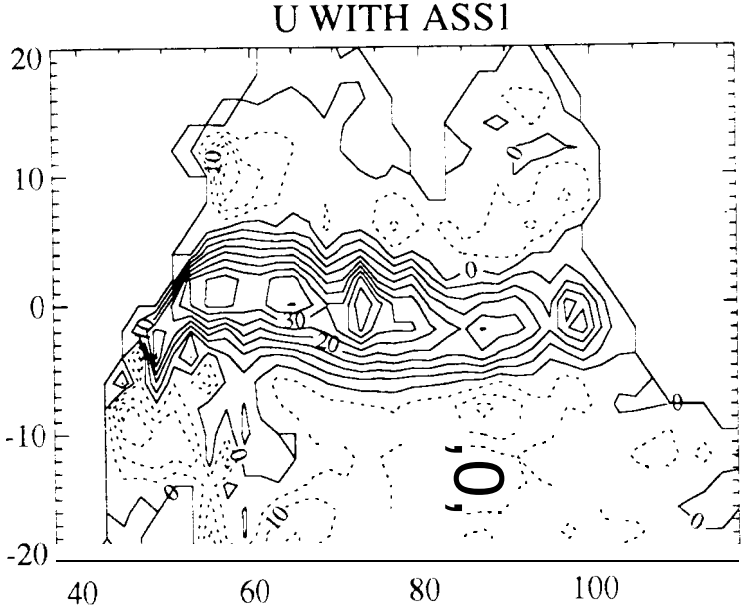
U WITH ASS1
20
10
0
-10
-20
40
60
80
100

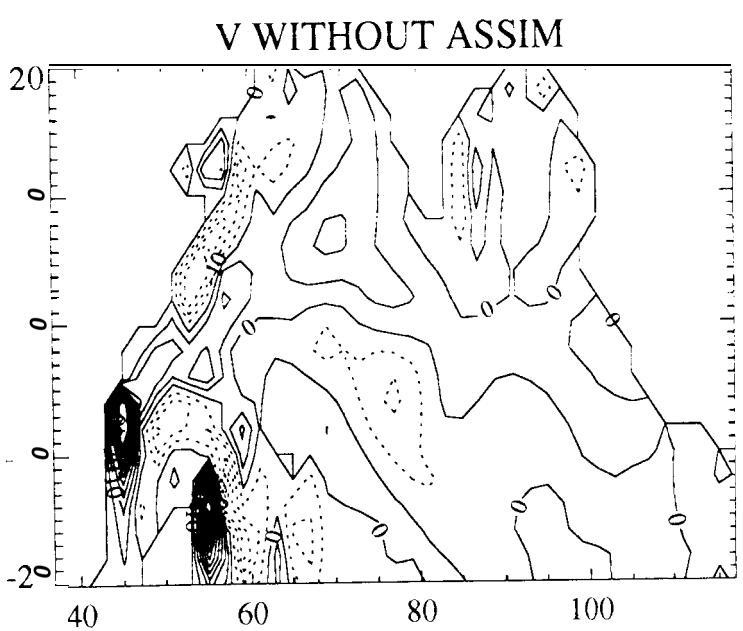
V WITHOUT ASSIM
20
0
0
0
-20
40
60
80
100

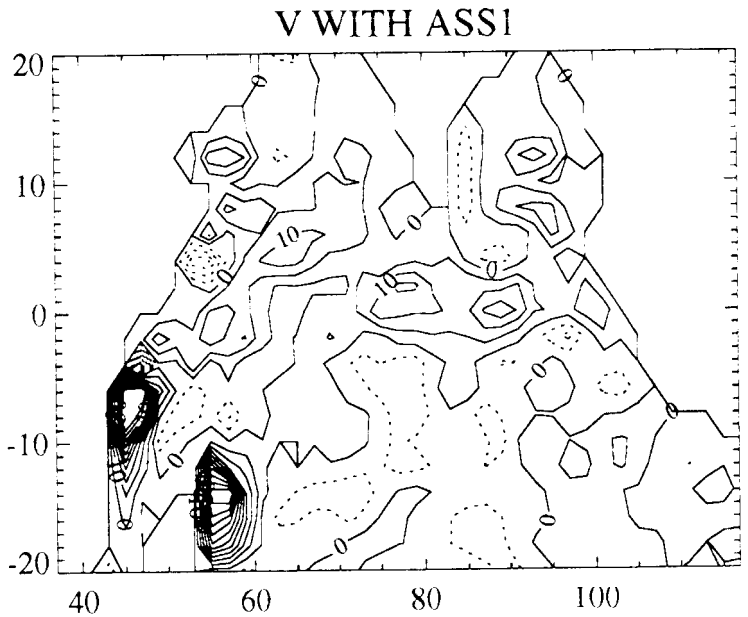
V WITH ASS1
20
10
0
-10
-20
40
60
80
100

Figure 12

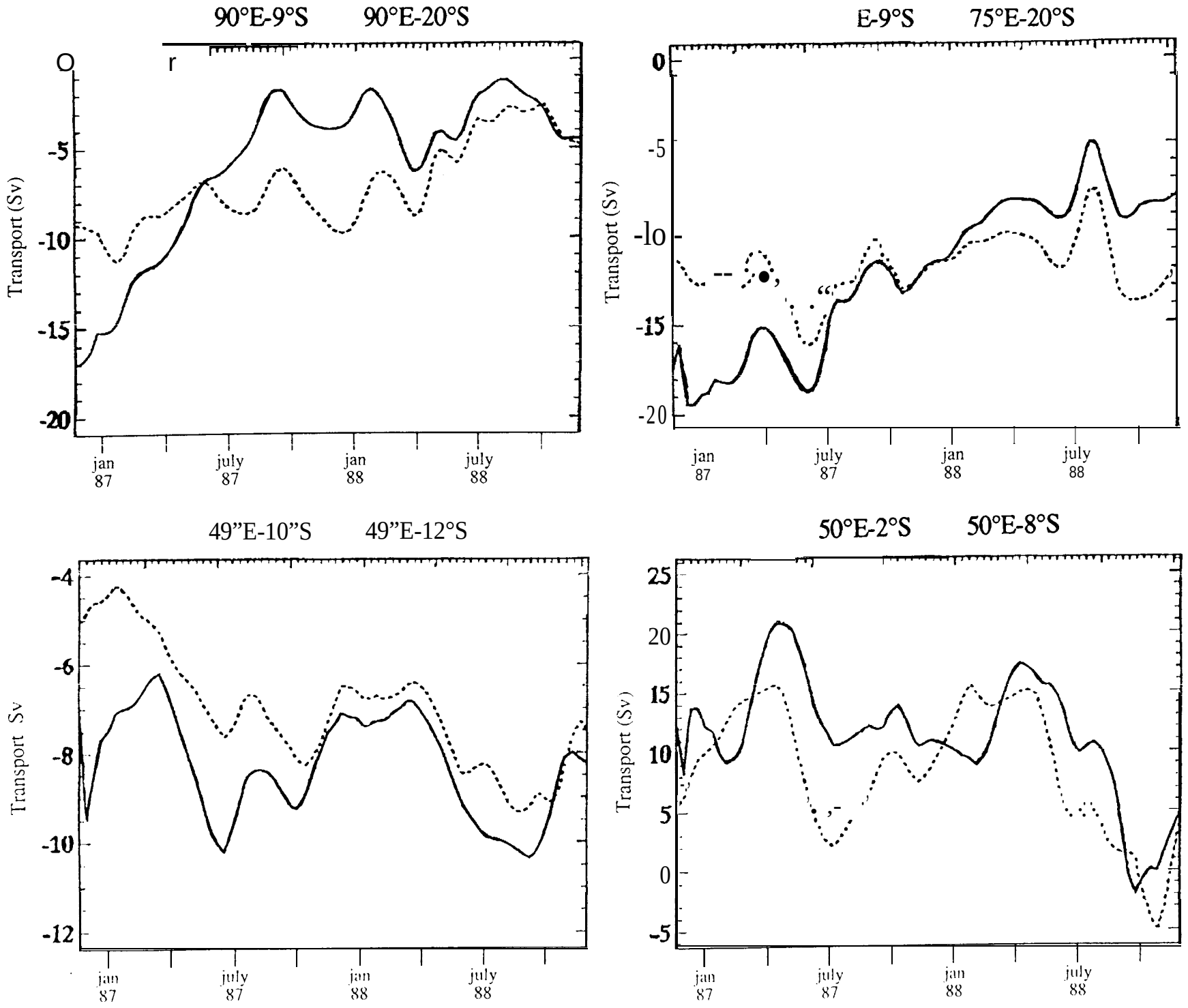

Figure 13abcd

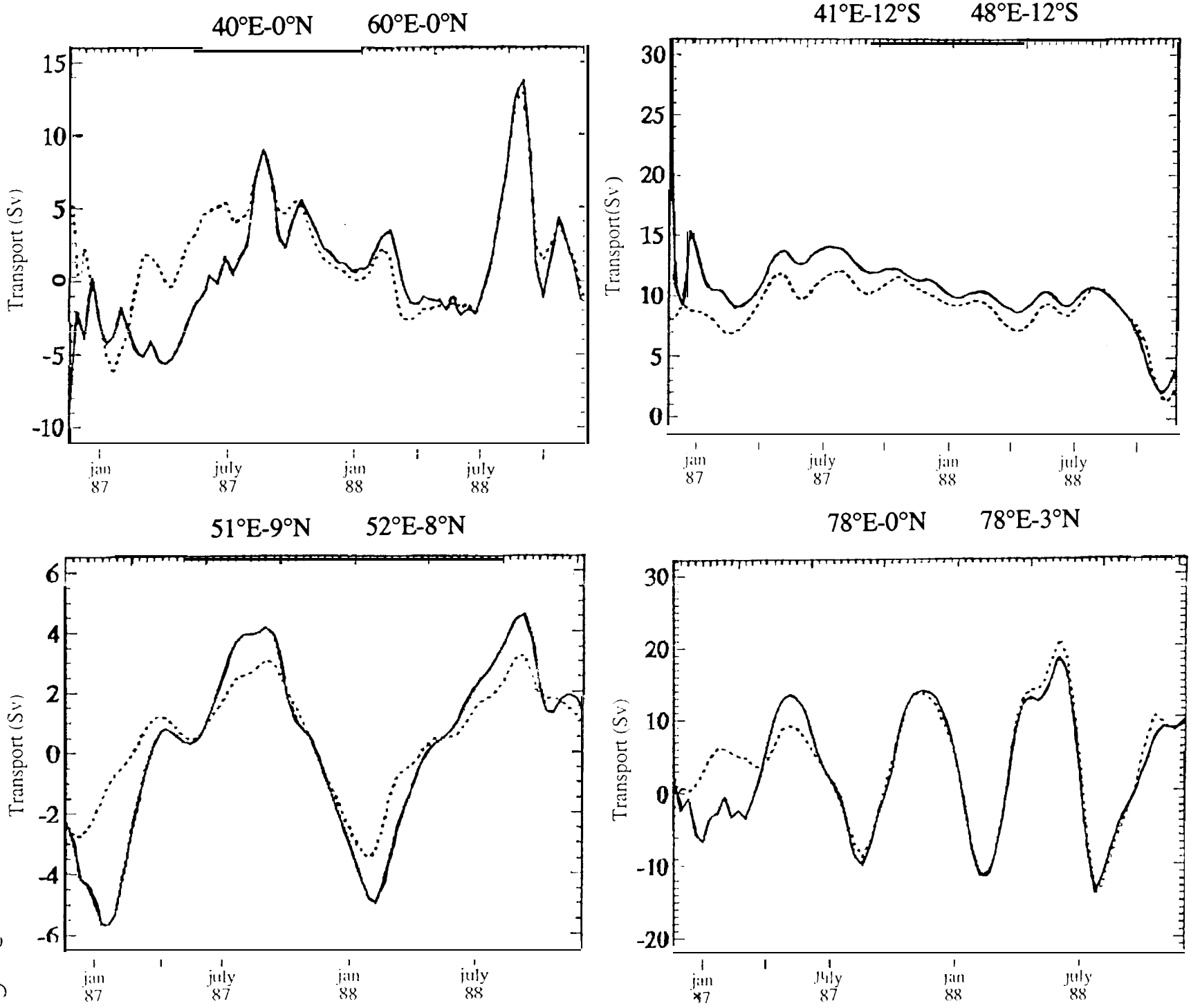

Figure 13 e f g h